Journal of South American Earth Sciences 104 (2020) 102897

Contents lists available at ScienceDirect

Journal of South American Earth Sciences

journal homepage: www.elsevier.com/locate/jsames

Thermochronological, petrographic and geochemical characteristics of the Combia Formation, Amagá basin, Colombia

Matthias Bernet [a,*], Juliana Mesa Garcia [b,c], Catherine Chauvel [a,d], Maria Jackeline Ramírez Londoño [b], Maria Isabel Marín-Cerón [b]

[a] Institut des Sciences de la Terre, CNRS, Université Grenoble Alpes, Grenoble, France
[b] Departemento de Geociencias, Universidad EAFIT, Medellín, Colombia
[c] present address: Geology Department, University of Michigan, Ann Arbor, MI, USA
[d] Université de Paris, Institut de Physique du Globe de Paris, CNRS, F-75005 Paris, France

ARTICLE INFO

Keywords:
Amagá basin
Combia formation
Subduction zone volcanism
Miocene volcanic activity
Northern Andes

ABSTRACT

The Amagá basin between the Western and Central Cordilleras of the Northern Andes of Colombia hosts the Neogene volcanic and volcaniclastic Combia Formation. Deposition of the Combia Formation in relation to Nazca plate subduction and arc volcanism is still a matter of debate. Therefore, the timing, petrography and geochemical characteristics of Combia Formation rocks were studied in the western and eastern parts of the Amagá basin, in order to gain more information on the type of magma generation and volcanic activity that led to the deposition of the Combia Formation.

Apatite and zircon fission-track dating largely confirm a 12-6 Ma age for the deposition of the Combia Formation. Petrographic and major element analyses show that mainly trachy-andesite ignimbrites with a calc-alkaline composition were deposited in the western Amagá basin, whereas the volcanic rocks of the eastern Amagá basin are lavas flow and fall-out deposits of basaltic andesites of tholeiitic affinity. Trace element and isotopic analyses show that slab dehydration and sediment melting/decarbonation were important in primary magma generation in the mantle wedge, but the primary magma was mixed with lower continental crustal melts (e.g. High-Pb radiogenic), resulting in characteristic isotope signatures in the western and eastern Amagá basin. Then, the hot-zone developed a high Pb-radiogenic, garnet-bearing lower continental crustal (LCC) level as a consequence of the quantity of dehydration of the subducting slab and of changes in the tectonic regime. An extensional pull-apart event (12- 9 Ma), likely facilitated rapid magma ascend to the uppermost crust along a subvertical magma plumbing system throughout the Romeral Fault zone in the eastern Amagá basin, and calc-alkaline magmas with adakite-like signature, which may indicate contractile tectonics that allow the formation of middle-to upper-crustal magma chambers with a garnet fractionation at depth and the evolution of silicate melts into the hot zone mainly related to the amount of water (>4 wt %) present.

1. Introduction

The late Paleogene to present-day magmatism of northwestern South America in Colombia can be divided into four major phases of activity at about 24–20 Ma, 12-6 Ma, 6-3 Ma, and 3 Ma to the Present (e.g. Sierra, 1994; Toro et al., 1999; Gonzalez, 2001; Ramírez et al., 2006; Cediel et al., 2011; Pérez et al., 2013; Lesage et al., 2013; Jaramillo et al., 2019). These different magmatic phases are related to the complex tectonic setting in which the Caribbean, Nazca and South American plates interact with each other (Fig. 1). The break-up of the Farallón plate into the Nazca and Cocos plates between 26 and 24 Ma (Marriner and Millward, 1984), the reorientation of subduction direction (Pardo-Casas and Molnar, 1987), and collision of the Panamá-Choco block with northwestern South America at about 25 Ma drove the first magmatic pulse (e.g. McCourt et al., 1984; Aspden et al., 1987; Kellogg and Vega, 1995; Trenkamp et al., 2002; Cediel et al., 2003; Lonsdale, 2005; Restrepo-Moreno et al., 2010; Farris et al., 2011). Second, since the late Paleogene the Nazca plate subduction zone was subjected to changes in subduction angle and direction over time, resulting in Miocene-Pliocene magmatic intrusions in the Western and Central

* Corresponding author.
E-mail address: matthias.bernet@univ-grenoble-alpes.fr (M. Bernet).

https://doi.org/10.1016/j.jsames.2020.102897
Received 1 April 2020; Received in revised form 7 September 2020; Accepted 10 September 2020
Available online 15 September 2020

Cordillera and deposition of the Combia Formation in the Amagá basin (e.g. Pardo-Casas and Molnar, 1987; Taboada et al., 2000; Cediel et al., 2003; Vargas and Mann, 2013). At the same time, subduction of the Caribbean plate beneath the northern (Caribbean) margin of South America caused isolated late Miocene-Pliocene volcanic activity in the Eastern Cordillera (e.g. Vargas and Mann, 2013), such as in the Vetas-California gold-mining district of the Santander Massif (Mantilla et al., 2013), or the Paipa-Iza complex 150 km to the north-east of Bogotá (Fig. 1; Pardo et al., 2005; Bernet et al., 2016). Today the main volcanic activity in Colombia is focused on the Central Cordillera with the Nevado del Ruiz, Nevado del Tolima, Cerro Machín, Nevado del Huila, Azufral, Cumbal, Galeras etc. well to the south of the study area (Fig. 1; e.g. Marín-Cerón et al., 2010, 2019; Leal-Mejía, 2011).

Different techniques have been used for more than a century to understand the genesis, age and evolution of the Combia Formation, including petrography, heavy mineral analysis, X-ray diffraction, geochemistry, geochronology, thermochronology and stratigraphic analyses (e.g. Grosse, 1926; Jaramillo, 1976; Calle and González, 1980; Álvarez, 1983; Marriner and Millward, 1984; Rios and Sierra, 2004; Pérez, 2005; López et al., 2006; Ramírez et al., 2006), but the evolution of the Nazca plate subduction zone magmatism still remains poorly constrained. Here we present a study of a suite of samples collected from three sections, the Cerro Amarillo section in the eastern Amagá basin, and the Anzá-Bolombolo and La Metida Creek sections in the western Amagá basin (Fig. 2), in order to improve the knowledge gained so far about the Combia Formation. The volcaniclastic, tuff/lapilli and flow deposits of the Combia Formation were studied with apatite fission-track (AFT) and zircon fission-track (ZFT) thermochronology, petrographic analyses, and major, trace element, Sr, Nd and Pb isotope analyses. All this was done with the objective of a) characterizing and comparing the eastern and western volcanic deposits, and b) to better understand the mid-late Miocene evolution of the Nazca subduction zone magmatism manifested between the Western and Central Cordilleras.

2. Geological setting

The Northern Andes of northwestern South America consist in Colombia of the Western, Central and Eastern Cordilleras (Fig. 1). Each of these mountain belts reflects a particular part of the long-term evolution of the Northern Andes, which is characterized by magmatic episodes since the Precambrian, during the Triassic, Jurassic, Late Cretaceous, and since the late Paleogene/Neogene until today (e.g. Aspden et al., 1987; Cediel et al., 2003). In general, these magmatic phases have been related to Farallón/Nazca plate subduction beneath the western margin of the South American plate (e.g. Marriner and Millward, 1984; McCourt et al., 1984; Cediel et al., 2003; Saenz, 2003; Restrepo-Moreno et al., 2009; Rodríguez et al., 2012). Accretion of tectonic blocks or terranes of oceanic affinity to the continental margin during the late Mesozoic and early Cenozoic did not cause Andean-type subduction volcanism, because of their relatively young age and high buoyancy preventing subduction (Cediel et al., 2003), and forcing surface uplift and the formation of the Western and Central Cordilleras during the Pre-Andean and Andean orogenies (e.g. van der Hammen, 1960; Taboada et al., 2000; Cediel et al., 2003).

The present-day Andean volcanism is commonly divided into four volcanic zones, the Northern Volcanic Zone (NVZ), Central Volcanic Zone (CVZ), Southern Volcanic Zone (SVZ), and Austral Volcanic Zone (AVZ) (Fig. 1A; Thorpe and Francis, 1979; Thorpe et al., 1982; Stern, 2004; Marín-Cerón et al., 2019). These segments have been distinguished based on differences in petrographic features and geochemical signatures, and they are separated from each other by volcanic gaps (e.g. Thorpe and Francis, 1979; Stern, 2004). The NVZ is located in north-western South America and encompasses the region of present-day volcanism in the Northern Andes of Ecuador and Colombia.

2.1. Geology of the Amagá basin

The Amagá basin forms the northern part of the much larger Amagá-Cauca-Patía basin located between the Western and Central Cordilleras of the Northern Andes in western Colombia (Fig. 1; Sierra and Marín-Cerón, 2011). Dextral strike–slip faulting along the Cauca and Romeral fault systems to the west and east respectively is responsible for development of the Amagá basin, which is tectonically a pull – apart basin (e.g. Cediel et al., 2003). Basin evolution started possibly during the Eocene (?) – Oligocene, with surface uplift and erosion of the Central Cordillera from the Late Cretaceous to Eocene and deposition of clastic sediments of the Lower Amagá Formation in the basin (e.g. Restrepo--Moreno et al., 2009). The Lower Amagá Formation is known for its quartz-rich sandstones and mainly sub-bituminous but locally anthracite grade coal (Silva et al., 2008; Blandon et al., 2008). The Lower Amagá Formation is separated from the Oligocene to Miocene Upper Amagá Formation by an unconformity and a change to a lithic arenite composition with sedimentary and metamorphic lithoclasts derived from the Central Cordillera (Paez Acuna, 2012). During the mid to late Miocene, subduction of the Nazca plate below the South American plate allowed the genesis of the Combia Formation in the Amagá basin (e.g. Grosse, 1926; Marriner and Millward, 1984; González, 2001; Cediel et al., 2003; Ramírez et al., 2006; Leal-Mejía, 2011; Cediel et al., 2011). Therefore, the Upper Amagá Formation is overlain by volcanic and volcaniclastic deposits of the Combia Formation. Here we focus on the Cerro Amarillo section in the eastern Amagá basin and the Anzá – Bolombolo and La Metida Creek sections in the western Amagá basin.

2.1.1. The Cerro Amarillo (CA) section

This section is located between the towns of Damasco and La Pintada (Fig. 2). It has a total thickness of 193 m and comprises 34 layers of welded tuff, pyroclastic and agglomerate breccia, lapilli tuff breccia, basaltic lava flows and scoria fall/flow deposits (Fig. 3). The layers vary in thickness from a 20 m pyroclastic and agglomerate breccia to 0.3 m lapilli tuff breccia, both at the top (Mesa-Garcia, 2015). There is also a 19.2 m thick welded tuff at the bottom. However, it is most common to find layers of 1–7 m in thickness. The layers are characterized by a tabular geometry. No evidence of pinch-out or lenses were observed in the outcrops (see supplementary data file). The bottom of the stratigraphic sequence is mainly characterized by lava flows and welded tuff, whereas the top of the sequence mainly consists of coarse to very coarse-grained pyroclastic flows. The bottom layers have on average a strike and dip of S05°E/25°SW. Towards the middle of the section the layers strike and dip N70°E/18°SE. Finally, the top breccia and lapilli tuff layers strike and dip N15°W/19SW. Many basalt and welded tuffs layers have randomly distributed vesicles and amygdules of variable sizes and shapes, some are elongated indicating lava flow directions.

2.1.2. The Anzá – Bolombolo (AB) section

This section is located on the western bank of the Cauca River (Fig. 2) between the villages of Anzá and Bolombolo. The stratigraphy of the 11.04 m thick succession consists of tuffs and lapilli tuffs in the lower part of the section, which are separated laterally from basaltic andesitic lava flows and ash flow deposits by an erosional unconformity (Fig. 4; Grosse, 1926; González, 2001; Sierra and Marín-Cerón, 2011). In the upper part of the sequence are a lapilli tuff breccia and a non-differentiated lava flow, which cover the underlying units and the unconformity. No particular sedimentary structures were observed at this location.

2.1.3. The La Metida Creek (MC) section

This section is located on the western bank of the Cauca River to the west of Bolombolo (Fig. 2). The Combia Formation crops out along the stream bed (e.g. González, 2001). The exposed stratigraphic sequence has a thickness of 45 m and is composed of 33 layers of tuff, lapilli tuff, lapilli tuff breccia, pyroclastic flows and volcano-clastic sandstones

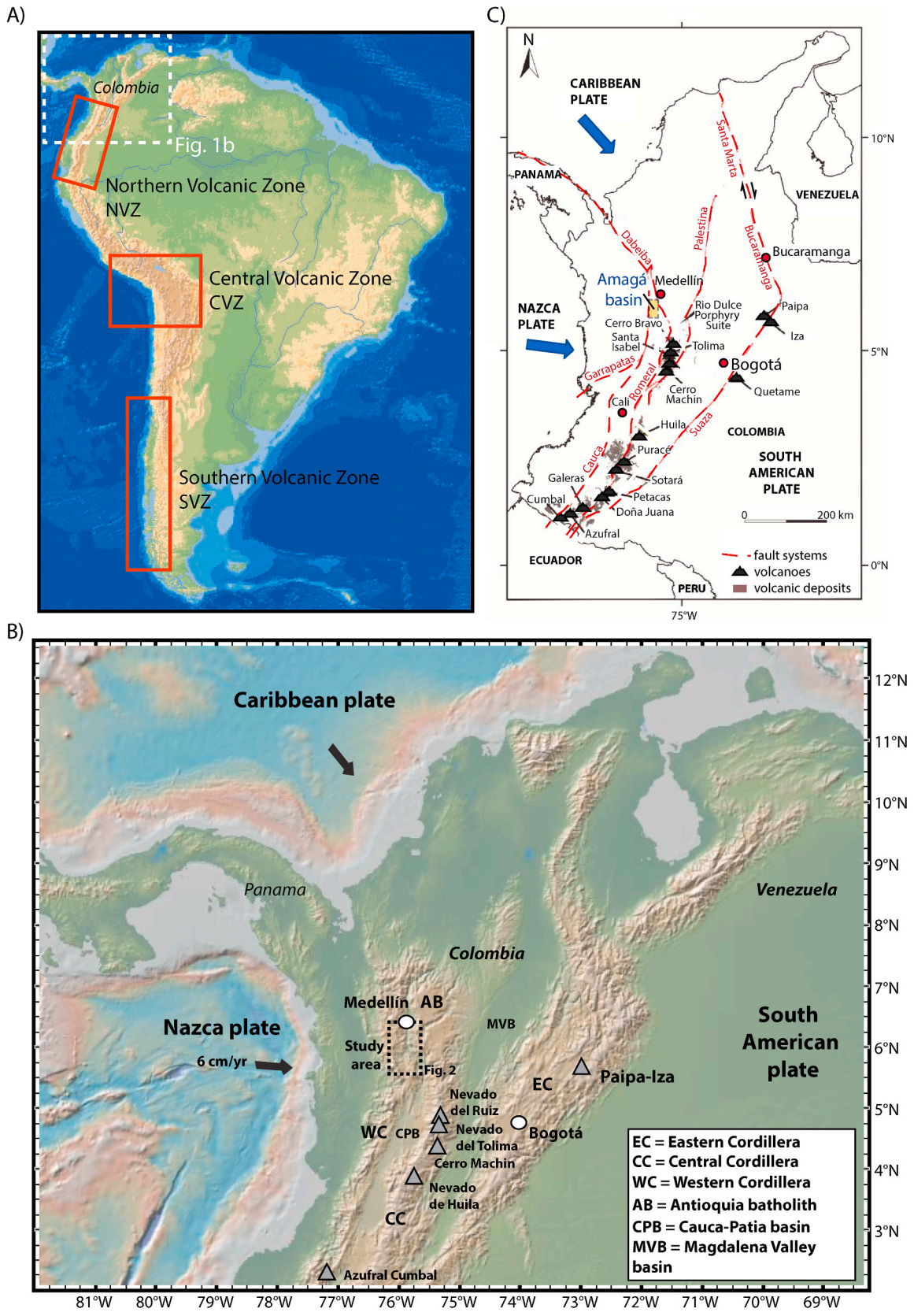

Fig. 1. A) Overview map of South America, showing the Norther Volcanic Zone (NVZ), Central Volcanic Zone (CVZ), and Southern Volcanic Zone (SVZ). B) Overview map of the Colombian Andes, showing the subduction of the Nazca and Caribbean plates beneath the South American plate. Also shown are the Western, Central and Eastern Cordilleras and areas of Pliocene to present volcanic activity, as well as the location of the study area (map from GeoMapApp, http://www.geomapapp.org/). C) Simplified tectonic sketch map of the Northern Andes of Colombia.

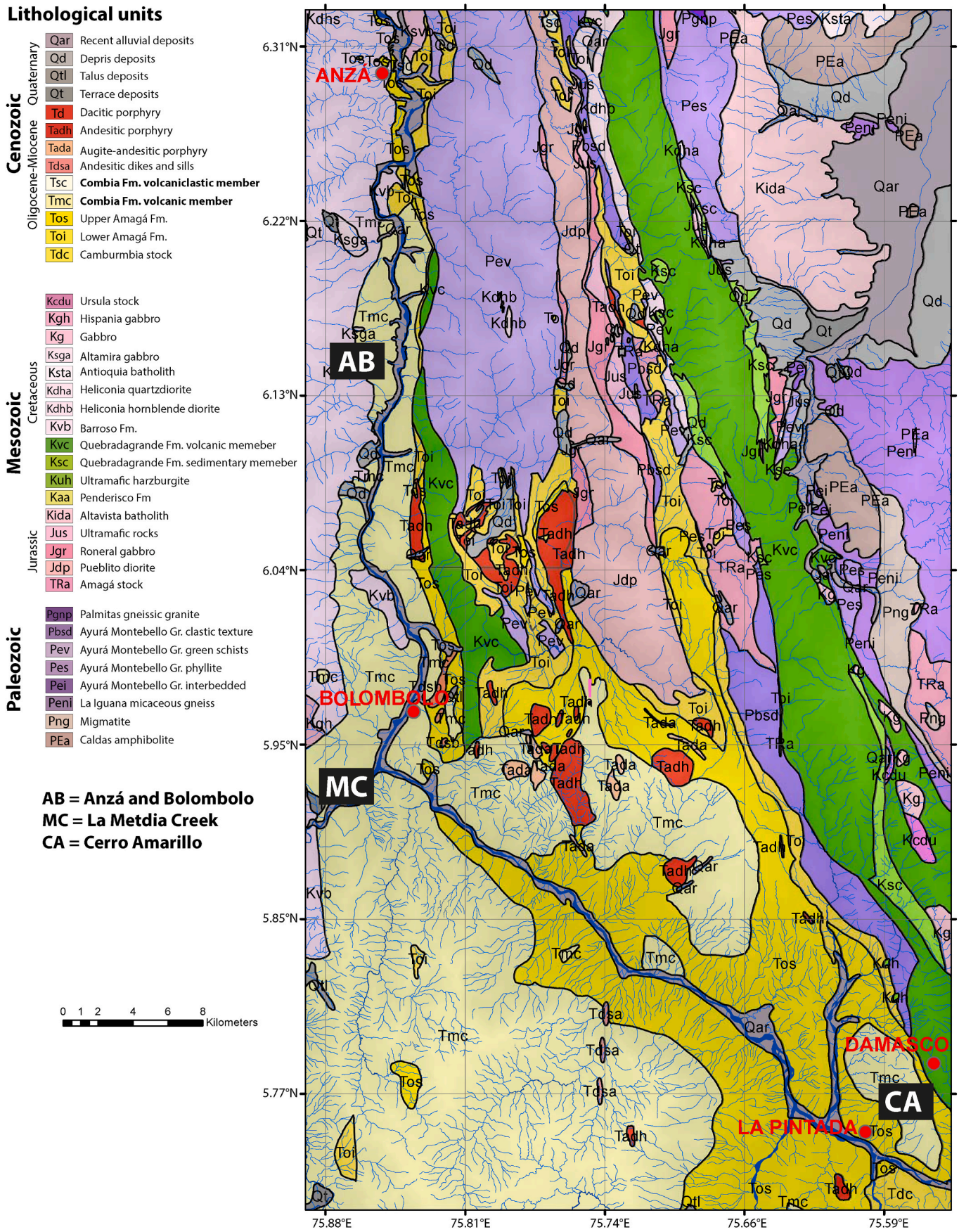

Fig. 2. Geological map of the Amagá basin with the locations of the Cerro Amarillo (CA), Anzá-Bolombolo (AB) and La Metida Creek (MC) sections (modified after Sierra and Marín-Cerón, 2011).

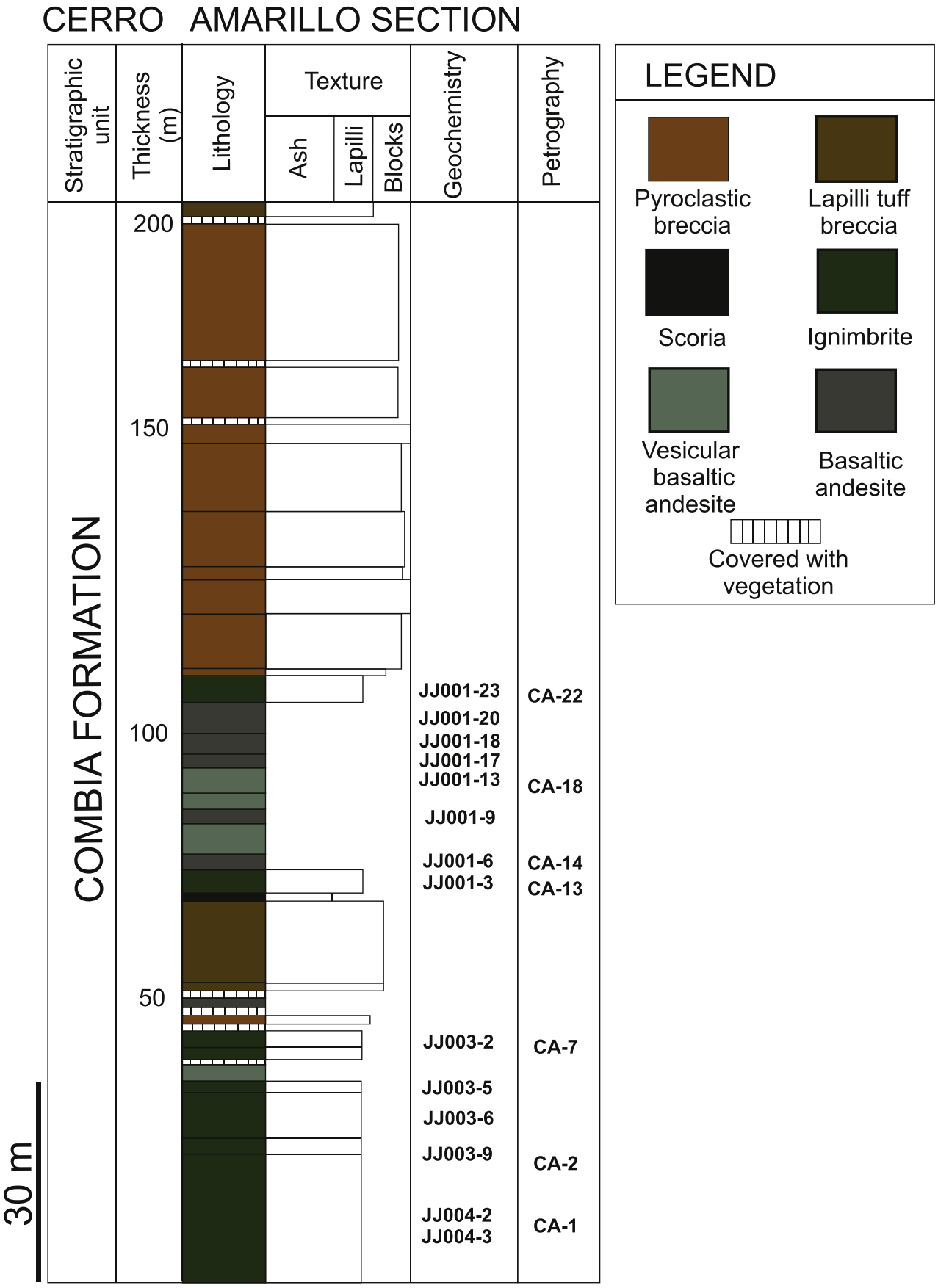

Fig. 3. Cerro Amarillo stratigraphic of the eastern Amagá basin.

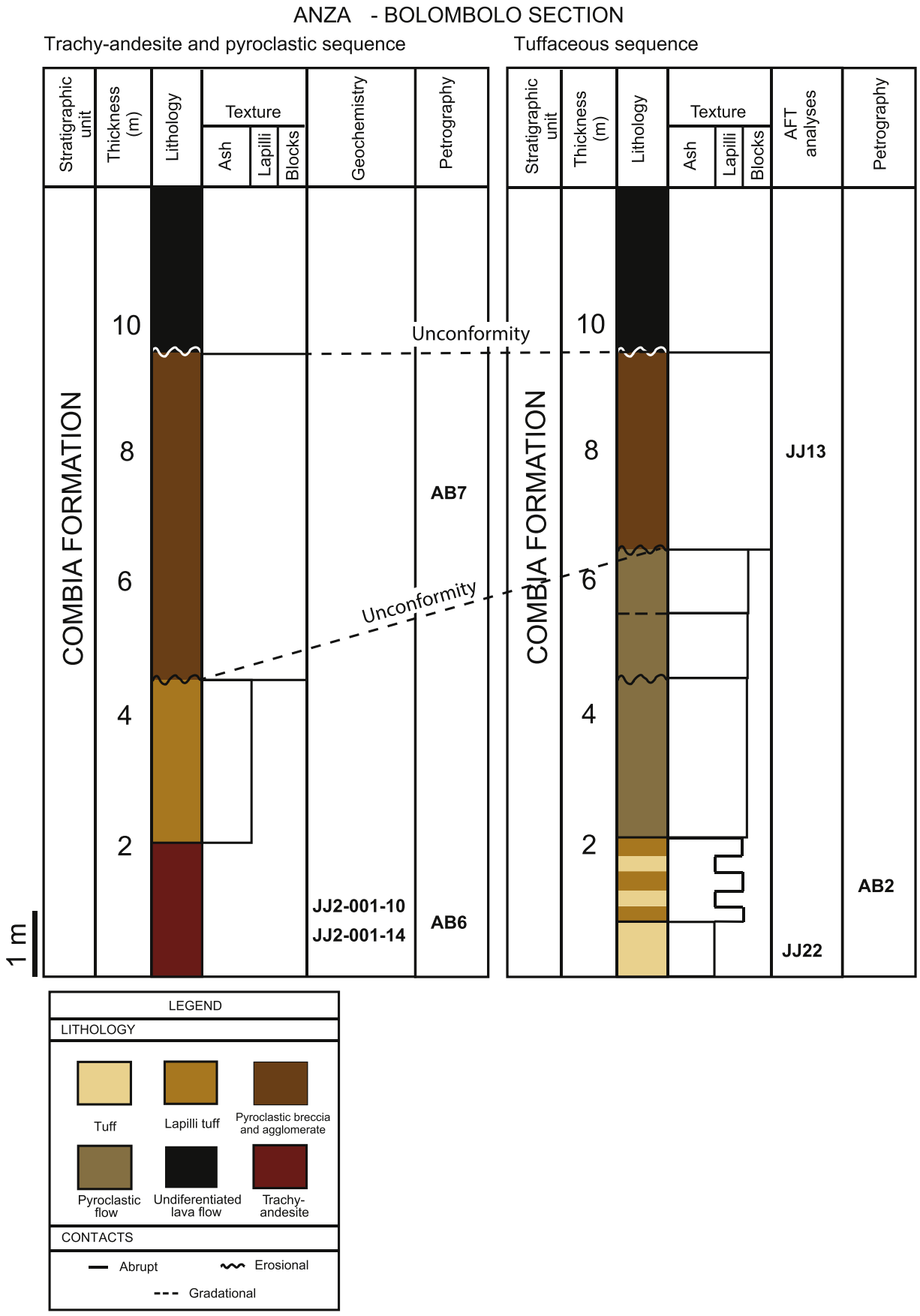

Fig. 4. Anzá Bolombolo stratigraphic section of the western Amagá basin.

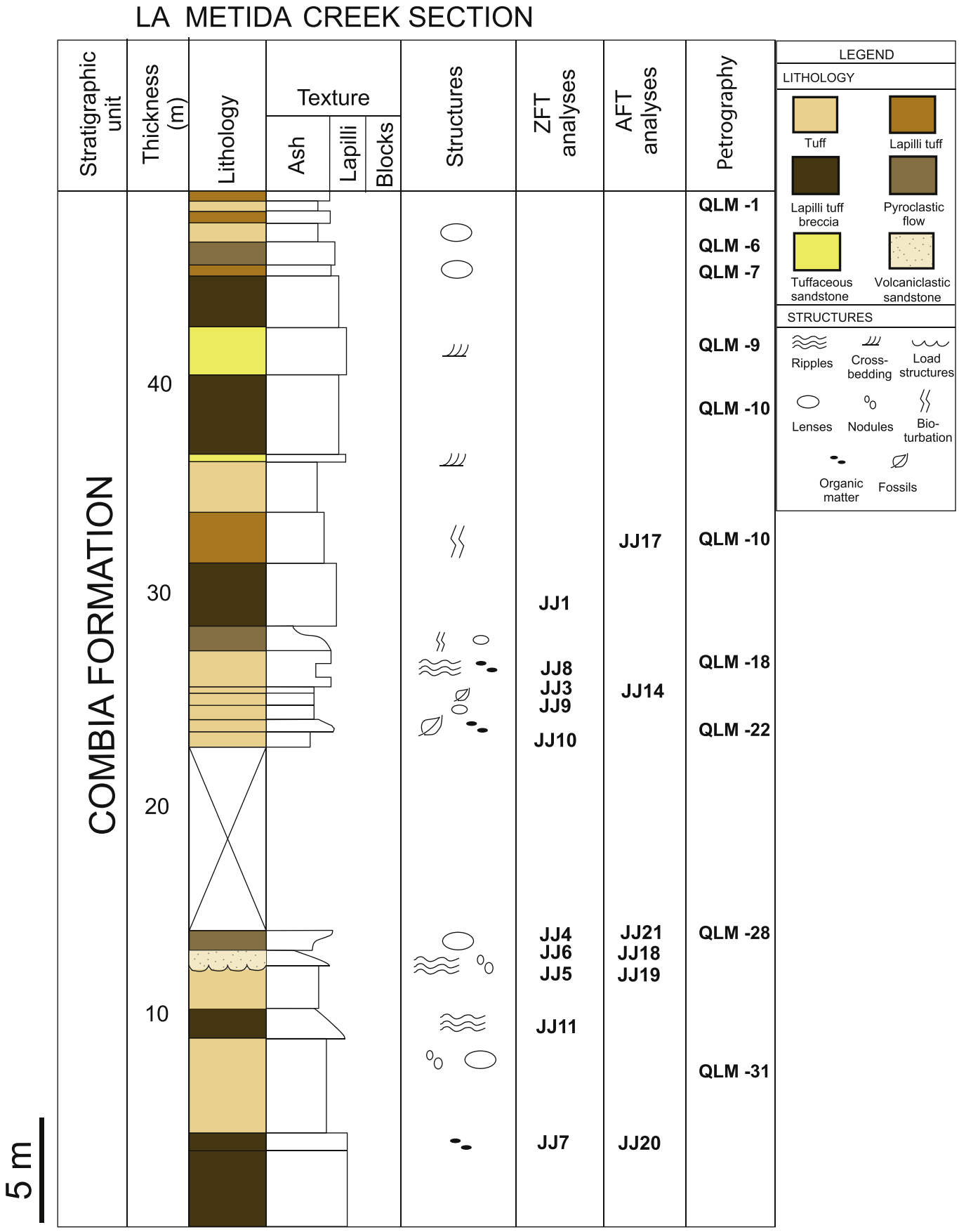

Fig. 5. La Metida Creek stratigraphic section of the western Amagá basin.

(Fig. 5). Sedimentary structures found throughout the sequence include lenticular bedding, load structures, ripple lamination and cross-bedding. The layers at the bottom are mainly grain-supported, whereas the top layers are matrix-supported. In addition, nodules and organic matter are commonly observed at the bottom of the section, and the middle section is characterized by bioturbation and fossilized plants (e.g. leaves). No such material was observed towards the top of the section.

3. Methods

3.1. Apatite and zircon fission-track analyses

AFT analysis was done on two samples from the Anzá-Bolombolo section and six samples from the La Metida Creek section. In addition, ten samples of the La Metida Creek section were analyzed with the ZFT method. Unfortunately, the apatite and zircon yield of the Cerro Amarillosection samples were too low for fission-track analyses.

Sample preparation and analyses were performed at the thermochronology laboratory of the Universidad EAFIT at Medellín and at the Institut des Sciences de la Terre (ISTerre) thermochronology laboratory at the Université Grenoble Alpes. Rock samples were crushed and sieved and heavy mineral fractions were separated using standard hydraulic, magnetic and heavy liquid separation techniques. The apatite crystals were mounted in epoxy and the zircon crystals in Teflon® sheets, polished and etched. Apatite grains were etched for 20 s at 21 °C with 5.5 mol HNO_3, and zircons were etched at 228 °C for 10–40 h in a NaOH–KOH melt to reveal fission tracks. A white mica sheet was mounted as the external detector. All samples were irradiated with thermal neutrons at the FRM II reactor in Garching, Germany, with a nominal fluence of 8×10^{15} n/cm^2 for apatite and 0.5×10^{15} n/cm^2 for zircon, together with IRMM540R dosimeter glasses and Durango age standards for apatite, and IRMM541 dosimeter glasses and Buluk and Fish Canyon Tuff age standards for zircon. After irradiation external detectors were etched in 48% HF for 18 min at 21 °C. Fission tracks were counted dry at 1250x using an Olympus BX51 microscope and the FTStage 4.04 system. Fission-track ages for each sample were calculated using the Binomfit software of Brandon (see Ehlers et al., 2005) and the RadialPlotter program of Vermeesch (2009).

3.2. Petrographic analyses

Petrographic analyses were performed on twenty samples, seven from the Cerro Amarillo section, three from the Anzá-Bolombolo section, and ten from the La Metida Creek section. Petrographic thin sections were prepared at Geoensayos S.A.S., Medellín, Colombia. Some of the pyroclastic samples had to be impregnated with epoxy, as these deposits were not well consolidated.

The samples were analyzed using an Olympus BX41TF petrographic microscope at the Geology department of EAFIT University. Modal analysis was performed counting 300–500 points per sample, using a point counter. The description of mineral assemblages and textures was done according to Mackenzie et al. (1984) and Ehlers (1987).

3.3. Geochemical analyses

The rock samples collected in the field were crushed to 1 mm chips at the Laboratory of Solid Materials at EAFIT University. Two hundred grams per sample were separated thoroughly, choosing the rock chips that were the least weathered and geochemical analyses for major and trace elements were performed in the clean laboratory (ISTerre) – Université Grenoble Alpes, France. Samples were finely powdered in an agate mortar previous to analyses, except for Pb isotope analysis for which rock chips were used directly. The sample preparation and analytical procedures were executed according to Chauvel et al. (2011), as summarized below.

For major elements, 50 mg of powdered sample were dissolved in 800 μl of concentrated HNO_3 and 15 drops of concentrated HF and heated in a Savillex beaker for 2 day at 90 °C on a hot plate. After cooling, 20 ml of H_3BO_3 (25 g/l) were added to the solution to neutralize excess HF, 10 g of HNO_3 and 250 ml of milliQ water for further dilution. Five standards (BR 24, BEN, BHVO2, AGV–1 and BCR–1), a duplicate and a blank were as well prepared for analysis. The solutions were analyzed using Inductively Coupled Plasma Atomic Emission Spectroscopy (ICP AES) at ISTerre to determine the major element composition of each sample. Concentrations were obtained using the international rock standard BR to calibrate the signal and the values recommended by Chauvel et al. (2011). Loss on ignition (LOI) was calculated for all samples by heating 1 g of sample at 1000 °C for 1 h.

Sixteen samples, five standards (BR 24, BEN, BHVO2, AGV–1 and BCR–1), three duplicates and one blank were analyzed for trace element contents. Major elements were obtained using an Inductively Coupled Plasma Atomic Emission Spectrometer (ICP-AES) and trace elements using an Inductively Coupled Plasma Mass Spectrometry (ICP MS) Agilent 7500 at ISTerre.

Ten samples were prepared for Nd, Pb and Sr isotope ratios analyses. Two sets of Sr samples, unleached and leached, were prepared following the same procedures as for the Nd samples and Pb samples, respectively. The samples were dissolved and conditioned in Savillex beakers. Rock chips were leached according to McDonough and Chauvel (1991), to eliminate as much as possible Sr and Pb superficial contamination. For Nd and unleached Sr isotopic measurements, 100 mg of sample were dissolved using HNO_3 and HF and isolated using the same procedure as Chauvel et al. (2011). For Pb and leached Sr, 1 g of rock chips was leached prior to dissolution using HCl and then isolated as in Chauvel et al. (2011). Nd and Pb isotopic ratios were measured using a Nu Plasma HR MC–ICPMS at ENS Lyon, France, while Sr isotopic ratios were measured using a Thermo Scientist Triton MS at the University of Brest, France.

4. Results

4.1. Fission-track results

4.1.1. Anzá – Bolombolo section

The tuff layer at the bottom of the Anzá-Bolombolo section (sample JJ22) has an AFT central age of 8.4 ± 3.1 Ma, and the pyroclastic flow sampled towards the top of the section (sample JJ13) has an AFT central age of 7.9 ± 1 Ma (Table 1; see the supplementary data for individual grain ages and radial plots of all samples). The combined Combia Formation AFT data are shown in a radial plot in Fig. 6A with a central age of 8.6 ± 1.4 Ma based on 302 grain ages. The radial plot is a common form of graphic representation of fission-track data. Every point reflects one single grain age.

4.1.2. La Metida Creek section

In total six samples were analyzed with the AFT method and ten with the ZFT method. AFT central ages range between 15.9 ± 11.1 and 5.1 ± 2.5 Ma. Nonetheless, inherited single grains with apparent cooling ages of between 374 and 49 Ma can also be observed in all samples (Table 1). Zircon crystals were mainly found in the middle and bottom of the La Metida Creek section. The euhedral to subhedral zircon crystals range in color from colorless, yellow, pink to red. The ZFT central ages are between 12.7 ± 2.4 Ma and 6.1 ± 1.1 Ma (Table 2). Except for the volcaniclastic sandstone sample (JJ6), no strong evidence exists of contamination with inherited zircons derived from surrounding country rock (see the supplementary data for individual grain ages and radial plots of all samples). The combined Combia Formation ZFT data are shown in Fig. 6B with a central age of 9.1 ± 1.1 Ma based on 346 grain ages.

Table 1
Apatite fission-track data of the Combia Formation.

Sample number	Lithology	Number of grains	Single grain age range (Ma)	RhoS ($x10^5$ t/ cm^2)	Ns	RhoI ($x10^5$ t/ cm^2)	Ni	RhoD ($x10^5$ t/ cm^2)	P (χ^2) (%)	Age dispersion (%)	Central age* (Ma) ±2 SE	U (ppm) ±2 SE
	AB section											
JJ13	Pyroclastic agglomerate	60	2.8–36.9	0.28	67	4.88	1183	9.72	44.9	2.7	7.9 ± 2.1	6 ± 0
JJ22	Tuff	35	3.2–38.5	0.29	35	4.96	592	9.72	36.3	24.0	8.4 ± 3.1	7 ± 1
	MC section											
JJ17	Lapilli – tuff	60	3.6–71.5	0.26	36	4.57	624	9.72	7.3	50.8	8.3 ± 3.1	6 ± 0
JJ14	Tuff	33	4.9–374.9	0.29	18	3.34	209	9.72	0.0	141.1	15.9 ± 11.1	4 ± 1
JJ21	Tuff	51	3.5–74.2	0.17	19	4.56	517	9.72	66.9	2.0	5.1 ± 2.5	6 ± 1
JJ18	Volcaniclastic sandstone	16	4.7–48.9	0.23	7	4.59	139	9.72	0.9	155.4	7.3 ± 9.4	6 ± 1
JJ19	Tuff	20	6.6–138.7	0.24	10	3.23	133	9.72	45.7	2.1	10.5 ± 7.3	4 ± 1
JJ20	Lapilli tuff breccia	27	4.9–138.5	0.50	28	5.68	317	9.72	6.9	57.1	15.8 ± 9.2	9 ± 1
combined		302	2.8–374.9					9.72	0.0	48.6	8.6 ± 1.4	6 ± 0

Note – RhoS: spontaneous track density. RhoI: induced track density; P(χ^2): Chi^2 probability. Fission-track ages were calculated using a Zeta value of 288.36 ± 7.90. AFT data calculated with Binomfit of Brandon (see Ehlers et al., 2005).

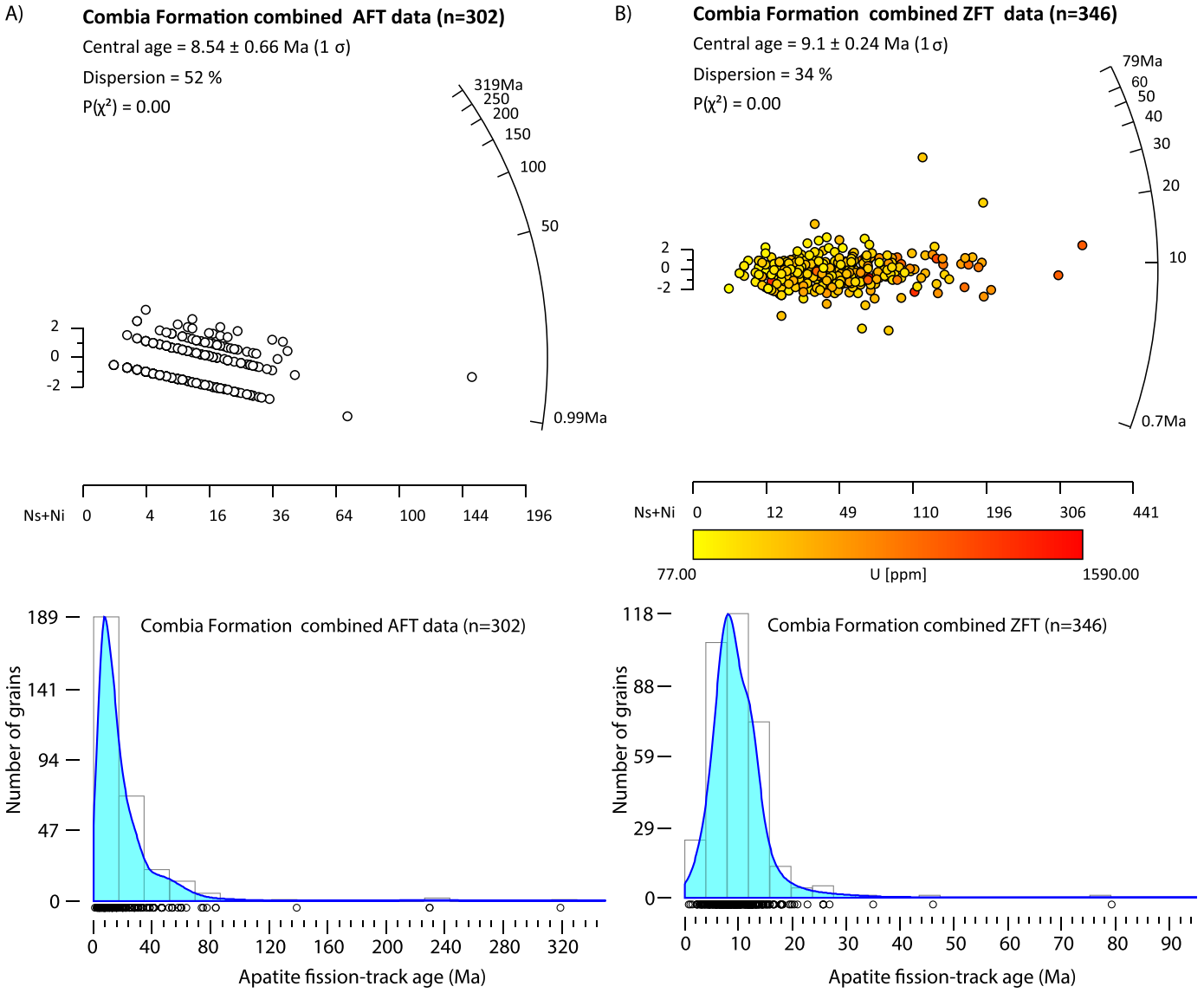

Fig. 6. Combia Formation combined fission-track data radial and Kernel Density function plots of A) apatite fission-track data radial plot and Kernel density estimate (KDE) plot. B) zircon fission track data with central ages radial plot and KDE plot. Radial plots of all individual samples are shown in the supplementary data. All plots were made with RadialPlotter of Vermeesch (2009).

Table 2
Zircon fission-track data of the La Metida Creek Formation.

Sample number	Lithology	Number of grains	Single grain age range (Ma)	RhoS ($x10^5$ t/cm^2)	Ns	RhoI ($x10^5$ t/cm^2)	Ni	RhoD ($x10^5$ t/cm^2)	P (χ^2) (%)	Age dispersion (%)	Central age* (Ma) ±2 SE	U (ppm) ±2 SE
JJ1	Lapilli tuff breccia	30	1.0–14.3	4.65	175	17.6	662	2.71	24.4	24.2	6.7 ± 1.5	258 ± 21
JJ8	Tuff	12	2.1–19.4	5.89	58	24.1	237	2.67	3.3	44.3	6.2 ± 2.6	359 ± 47
JJ3	Tuff	25	4.0–19.5	10.6	383	27.5	993	2.71	47.5	6.6	10.0 ± 1.7	405 ± 28
JJ9	Tuff	28	0.9–25.5	13.2	570	33.1	1432	2.67	0.0	35.3	10.1 ± 2.1	493 ± 29
JJ10	Tuff	22	5.0–20.0	10.5	363	28.6	989	2.66	68.0	0.6	9.3 ± 1.5	427 ± 29
JJ4	Tuff	31	2.9–25.8	17.7	585	38.8	1280	2.70	0.3	24.1	11.2 ± 2.0	572 ± 36
JJ6	Volcaniclastic sandstone	51	2.9–46.7	10.6	909	22.1	1844	2.69	0.0	44.1	12.7 ± 2.4	327 ± 17
JJ5	Tuff	31	2.6–14.8	14.1	515	3.85	1405	2.69	73.1	6.5	9.4 ± 1.4	569 ± 14
JJ11	Lapilli tuff breccia	48	1.3–16.1	6.27	362	2.63	1517	2.65	14.2	19.6	6.1 ± 1.1	394 ± 22
JJ7	Lapilli tuff breccia	68	4.3–14.8	9.00	824	29.5	2705	2.68	94.0	0.7	7.8 ± 1.1	439 ± 20
Combined		346	0.9–46.7	10.2	4744	28.5	13,206	2.68	0.0	33.9	9.1 ± 1.1	418 ± 14

4.2. Petrographic results

4.2.1. Cerro Amarillo section

In general, the seven samples analyzed for this section share similar characteristics being hypocrystalline, porphyritic rocks. The mineral assemblage is represented by plagioclase + pyroxene ± amphibole ± olivine (Table 3). Other minerals present in the samples are secondary calcite, biotite and opaque minerals. The xenoliths found in the ignimbrites are mainly basalts (aphanitic textures and volcanic glass) or andesites (plagioclase crystals in volcanic glass). Some of these fragments are fractured. There is also evidence of oxidation and sericitization, even though carbonate minerals are the main alteration product in these samples.

The ignimbrites are dominated by crystals and rock fragments ranging from 55 to 70%, whereas the two basalt samples have different percentage relationships between the matrix and phenocrysts, CA – 14 rich in crystals and CA – 18 rich in matrix. The crystal and/or rock fragments are inequigranular, which is observed in the presence of seriate, glomeroporphyritic, poikilitic, and interstitial textures. Overgrowth textures such as skeletal, corona and crystal zoning are also found in the samples, mainly in the ignimbrites. The crystals have subhedral to anhedral shapes in most samples; euhedral-shaped crystals are rare or unable to identify due to alteration. The matrix is generally altered to secondary calcite, but in some cases a non-altered volcanic glass composition is observed with some embedded microlites of plagioclase and less common pyroxene. Color plates of thin section

Table 3
Petrographic modal analyses.

CA section	CA - 1	CA – 2	CA – 7	CA – 13	CA - 14	CA - 18	CA - 22			
Plagioclase	48.61	19.1	36.2	9.25	32.1	89.7	31.2			
Hypersthene	–	42.2	23.5	51.2	47.2	10.3	21.8			
Augite	13.19	4.7	3.2	9	9.89	–	9.5			
Hornblende	3.47	0.6	–	–	–	–	5.4			
Calcite	9.03	1.3	–	–	7.58	–	5.01			
Olivine	5.21	–	–	–	–	–	8			
Biotite	–	0.5	0.32	1	3.23	–	1.6			
Sericite	–	–	3.5	–	–	–	–			
Rock fragments	19.8	19.4	28.6	29.55	–	–	17.49			
Oxides	–	8.8	4.8	–	–	–	–			
Opaque minerals	0.69	3.4	–	–	–	–	–			
Total	100	100	100.12	100	100	100	100			
AB section	AB – 2	AB – 6	AB – 7							
Plagioclase	57.14	69.13	52.22							
Pyroxene	42.86	12.01	29.1							
Spherulites	–	9.86	18.68							
Olivine	–	9	–							
Total	100	100	100							
MC section	QML - 1	QML – 6	QML - 7	QML – 9	QML – 10	QML - 14	QML - 18	QML - 22	QML - 28	QML - 31
Plagioclase	71.22	61.4	55	40	57.14	85	57.5	62.5	60	77.14
Pyroxene	–	10.53	15	20	22.85	7.6	25	25	25	14.29
Hornblende	5.91	5.26	5	–	–	2.4	–	–	–	–
Biotite	0.33	–	–	–	–	–	–	–	–	–
Oxides	2.13	–	–	5.71	5.72	5	–	12.5	15	8.57
Rock fragments	16.48	15.79	–	8.57	–	–	–	–	–	–
Opaque minerals	3.94	7.02	25	25.72	14.29	–	–	–	–	–
Spherulites	–	–	–	–	–	–	17.5	–	–	–
Total	100.01	100	100	100	100	100	100	100	100	100

photographs are given in the supplementary data archive.

4.2.2. Anzá – Bolombolo section

The analyzed samples are hypocrystalline, inequigranular volcanic rocks. The mineral assemblages are mainly plagioclase + pyroxene (Table 3). The matrix consists of volcanic glass. Other rock components are spherulites, found in samples AB–6 and AB–7, and olivine, found in sample AB–6. These samples are located to the east of the unconformity described in the stratigraphic section. The samples are characterized by having skeletal and crystal zoning overgrowth, spherulites and vesicular textures. Color plates of thin section photographs are given in the supplementary data.

4.2.3. La Metida Creek section

Nine samples from this section are tuff deposits and only one sample (QML – 9) is a tuffaceous sandstone because of the presence of cross-bedding in the layer. Petrographic characteristics of all samples are similar and the classification as pyroclastic and epiclastic rocks is based on sedimentary structures observed in the field. The mineral assemblage is mainly plagioclase + pyroxene. Some amphiboles are present in the bottom layers.

The sampled rocks are mainly hypocrystalline due to the presence of phenocryst, and microlites in the matrix. The minerals have inequigranular and seriate fabrics. In general, skeletal textures are found in all analyzed samples. Other common textures are glomero-porphyritic and crystal zoning, although the latter is not present in the samples analyzed from the middle section of the La Metida Creek section. Similar to the Anzá-Bolombolo section spherulites are found in the samples from the bottom layers. Color plates of thin section photographs are given in the supplementary data.

4.3. Geochemical results

Mayor element analyses of 16 samples are presented in Table 4. Loss on ignition (LOI) is generally below 3 wt%. For the Cerro Amarillo section samples, SiO_2 contents range between 51 and 53 wt%. The sample plot in the tholeiitic field of the AFM diagram (Fig. 7A) and correspond to basaltic andesite according to Fig. 7B. Samples coming from the Anza-Bolombolo area have slightly higher SiO_2 content at about 56 wt%, plotting in the alkaline field in Fig. 7A and correspond to trachy-andesites in Fig. 7B. In the SiO_2 vs K_2O diagram of Peccerillo and Taylor (1976) the Cerro Amarillo samples plot in the High-K Calc-Alkaline Series field (Fig. 8).

Trace element contents of all samples are given in Table 5 and plotted in primitive mantle-normalized spider diagrams in Fig. 9A. The Cerro Amarillo samples display an enrichment in large-ion lithophile elements (Rb, Ba, Cs, Sr) and a strong depletion in Nb and Ta. The Anzá-Bolombolo samples are even more enriched in Rb, Ba, Cs and Sr, and with similar depletion in Nb and Ta (Fig. 9A). Next to the difference in large-ion lithophile elements (LILE) and Light Rare Earth Elements (LREE), the main difference between the Cerro Amarillo and Anzá-Bolombolo samples is the Li enrichment of the Anzá-Bolombolo section samples. Samples from both sections are enriched in LREE relative to the Heavy Rare Earth Elements (HREE) (Fig. 9B). The Cerra Amarillo section samples are weakly fractionated, compared to the moderately fractionated Anzá-Bolombolo section samples. No significant Eu anomaly exists for all samples. Note also the spoon-like spectra for AB samples. This can usually be ascribed to amphibole fractionation.

Nd, Sr, and Pb isotope analyses of all samples are given in Table 6. Strontium isotopic ratios measured on leached and unleached samples are similar within errors. $^{87}Sr/^{86}Sr$ ratios range from 0.703862 to 0.703931 for the Cerro Amarillo section samples, but are higher at about 0.70417 for the Anzá-Bolombolo section samples (Fig. 10A). $^{143}Nd/^{144}Nd$ ratios vary between 0.51292 and 0.51298 for the Cerro Amarillo section samples, and are somewhat lower at 0.51290 for the Anzá-Bolombolo section samples (Fig. 10B and C). Finally, the Cerro Amarillo section samples define a small range in Pb isotopic ratios ($^{208}Pb/^{204}Pb$: 38.68 to 38.80, $^{207}Pb/^{204}Pb$: 15.61 to 15.62 and $^{206}Pb/^{204}Pb$: 18.91 to 19.07), and the Anzá Bolombolo section samples fall in the middle of the range (Fig. 11a and b; Table 7).

5. Discussion

5.1. Constraints from low-temperature thermochronology

The AFT and ZFT data presented in this study can in principle be used for constraining the age of deposition of the volcanic and volcaniclastic deposits of the Combia Formation (Kowallis et al., 1986; Bernet et al., 2016). The AFT and ZFT data central age values ranging from 15.9 to 5.1 Ma for AFT and 12.7–6.1 Ma for ZFT, bracket the known zircon U–Pb 12-6 Ma age of Combia Formation volcanic activity (e.g. Leal-Mejía, 2011; Jaramillo et al., 2019). Our fission-track data highlight two important aspects that are challenging in dating relatively young volcanic and volcaniclastic deposits with the fission-track method. As to be expected the ZFT data correspond more closely to the known 12-6 Ma age range determined from zircon U–Pb analyses (Leal-Mejía, 2011; Jaramillo et al., 2019), because of the higher U concentration and the better track counting statistics resulting in higher precision results. The U concentration of the apatites in the Combia Formation are in general very low (<10 ppm), resulting in lower precision AFT ages. As can been seen in the single grain data provided in the supplementary data archive, many apatite grains are zero-track grains, resulting in a very high single grain age uncertainty, as the induced track counts also tend to be low because of the very low U concentrations.

In addition, dealing with volcanic and particularly volcaniclastic deposits the risk of contamination with apatites and zircons recycled from the country rock is high, and has been shown to be the case for certain volcanic deposits of the Paipa-Iza volcanic complex (Bernet et al., 2016). Here we also think that zircons with >12 Ma apparent cooling ages were most likely recycled from the Amagá Formation

Table 4
Major elements (wt %) of the Cerro Amarillo and Anzó – Bolombolo section samples.

Oxides (wt %)	JJ1 - 3	JJ1 - 6	JJ1 – 9	JJ1 - 13	JJ1 - 17	JJ1 – 18	JJ1 - 20	JJ1 - 23	JJ3 – 2	JJ3 - 5	JJ3 - 6	JJ3 - 9	JJ4 - 2	JJ4 - 3	JJ2-1-10	JJ2-1-14
SiO_2	53.20	52.68	52.56	52.62	52.55	52.10	52.49	52.64	52.09	51.19	52.07	52.22	51.78	52.34	55.45	55.78
Al_2O_3	14.80	14.70	14.82	14.71	14.66	14.61	14.59	14.87	18.30	15.29	15.05	15.22	17.49	17.66	19.02	18.93
Fe_2O_3 t	12.03	11.77	12.13	12.82	12.67	12.55	12.93	12.75	10.40	13.44	13.48	13.63	10.49	10.23	5.01	5.53
MnO	0.19	0.17	0.17	0.19	0.19	0.18	0.19	0.18	0.18	0.21	0.21	0.21	0.17	0.17	0.09	0.09
MgO	3.56	3.51	3.32	3.48	3.43	3.32	3.49	3.30	2.99	3.44	3.50	3.46	3.48	3.05	1.05	1.12
CaO	7.68	7.82	7.56	7.57	7.58	7.47	7.36	7.50	9.33	8.28	8.35	8.24	8.80	8.84	4.51	5.28
Na_2O	2.95	2.74	2.63	2.60	2.69	2.70	2.76	2.80	2.66	2.76	2.89	2.80	2.94	2.98	3.58	3.73
K_2O	1.89	1.75	1.94	1.88	1.98	1.84	1.79	1.82	1.20	1.40	1.25	1.45	1.47	1.48	3.58	4.60
TiO_2	1.31	1.30	1.38	1.39	1.38	1.38	1.38	1.38	0.86	1.03	1.06	1.06	0.96	0.99	5.10	0.52
P_2O_5	0.48	0.48		0.50	0.50	0.51	0.52	0.51	0.28	0.39	0.39	0.39	0.44	0.46	0.47	0.49
LOI	1.48	2.75	2.60	2.19	1.77	1.98	1.47	1.74	1.12	1.63	1.63	1.65	2.08	2.31	5.18	2.70
SUM	99.67	99.11	99.95	99.4	98.64	98.97	99.49	99.41	99.06	99.88	100.33	100.1	100.51	98.45	98.77	99.67

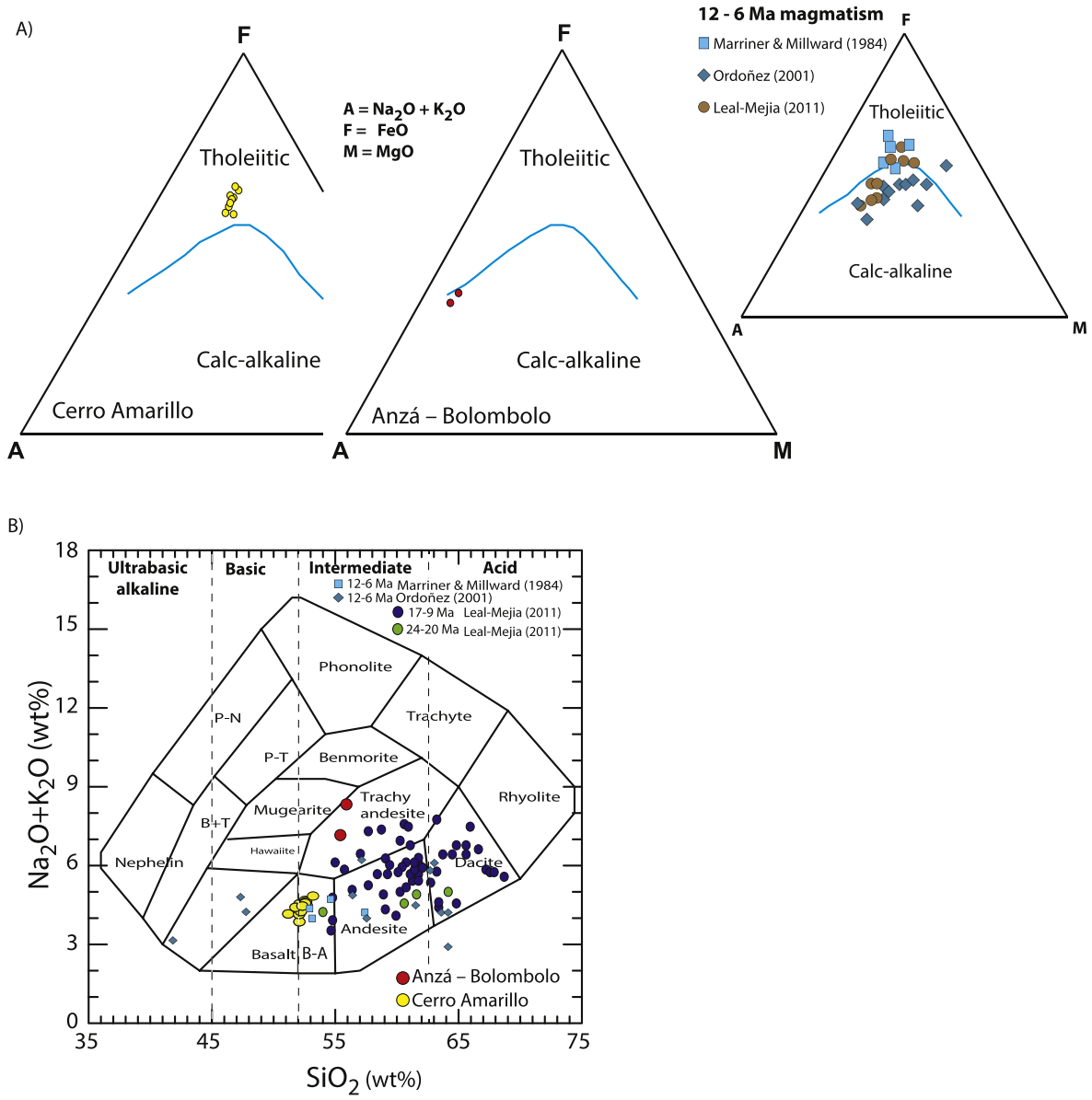

Fig. 7. A) AFM diagram plot (Irvine and Baragar, 1971) for volcanic rocks from the Cerro Amarillo and Anzá- Bolombolo sectionsData of Marriner and Millward (1984), Ordoñez (2002) and Leal-Mejía (2011) from the Combia Formation are also shown for comparison. B) Total alkalis versus silica (TAS) diagram of volcanic rocks from the Cerro Amarillo and Anzá Bolombolo sections; boundaries in the total alkalis are from LeMaitre et al. (1989) for rock classification Data of Marriner and Millward (1984), Ordoñez (2002) and Leal-Mejía (2011) are shown for comparison. B-A = Basaltic Andesite, P-T = Phonolitic Tephrite, P–N = Phonolitic Nepheline, B + T = Basanite and Tephrite.

(Piedrahita et al., 2017). Pre-Miocene cooling ages are common in apatites of the Combia Formation deposits (Table 1), and are considered to be derived from underlying basement rock and recycling of the Amagá Formation.

In summary, based on the AFT and ZFT data, volcanic activity occurred between 12 Ma and 6 Ma. The main phase of activity for these deposits may have been at around 9 Ma, as suggested by the central ages of the combined AFT and ZFT data sets shown in Fig. 6. This confirms a late Miocene depositional age, which has previously been proposed based on stratigraphic position and whole rock K–Ar dating of hypabyssal porphyries (e.g. Grosse, 1926; Restrepo et al., 1981; Marriner and Millward, 1984; González, 2001; Pérez, 2005; Ramírez et al., 2006; Leal-Mejía, 2011).

5.2. *Shallow-level processes prior to eruption*

In general, the rocks have porphyritic textures, and plagioclase is one of the main mineral components, both as phenocrysts and microlites. Similar results have been reported by several authors (e.g. Marriner and Millward, 1984; López et al., 2006; Ramírez et al., 2006; Bissig et al., 2017; Jaramillo et al., 2019).

The matrix for most samples is comprised of volcanic glass with microlites of plagioclase and to a lesser extent pyroxene. Devitrification of the volcanic glass matrix is common in the samples. The samples show evidence of alteration (e.g. secondary calcite, oxidation, argillitization) which may indicate metasomatic to shallow processes related to hydrothermal alterations and mineralization processes in the hypabyssal porphyries of the study area (e.g. Tassinari et al., 2008; Leal-Mejía, 2011; Lesage et al., 2013; Uribe-Mogollón, 2013).

All samples show disequilibrium textures such as skeletal, sieve and

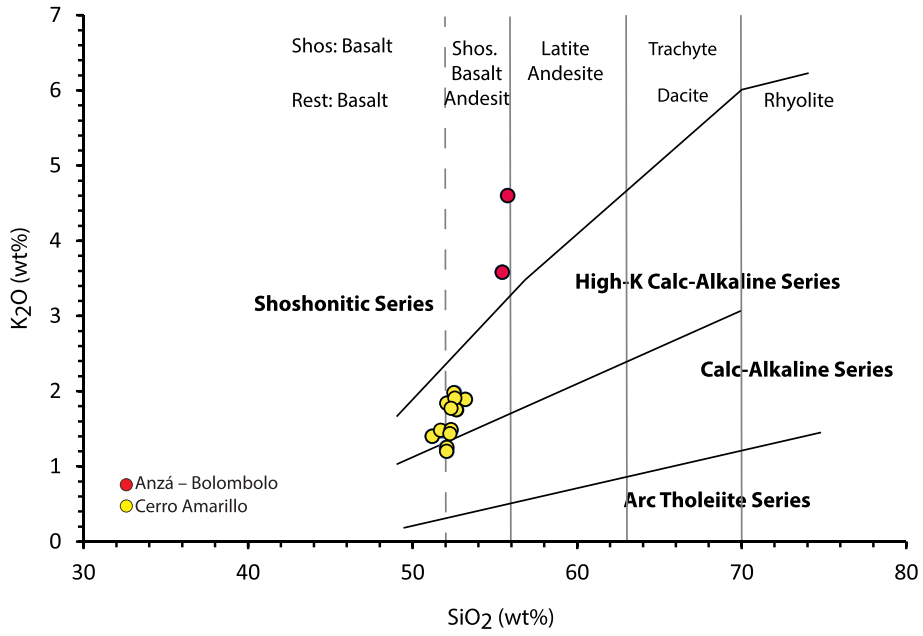

Fig. 8. SiO_2 vs K_2O diagram of Peccerillo and Taylor (1976). The Cerro Amarillo samples plot in the High-K Calc-Alkaline Series field and the Anzá Bolombolo samples in the Shoshonitic Series field.

Table 5
Trace elements (ppm) of volcanic rock samples of the Cerro Amarillo and Anzó Bolombolo sections.

	JJ1-3	JJ1-6	JJ1-9	JJ1-13	JJ1-17	JJ1-18	JJ1-20	JJ1-23	JJ3-2	JJ3-5	JJ3-6	JJ3-9	JJ4-2	JJ4-3	JJ2-1-10	J22-1-14
Li	8.52	8.33	7.58	8.46	8.73	9.75	8.71	10.4	8.98	8.76	7.64	9.39	8.07	8.38	13.6	15.5
Sc	31	30.7	30.2	30.5	30.1	29.5	30.1	30.4	27.4	33	32.8	33.1	24	24.8	8	8.75
Ti	7840	7760	8270	8340	8210	8110	8250	8240	5070	6170	6160	6200	5690	5900	2710	3020
V	343	340	367	369	361	365	366	367	296	331	338	337	268	278	96.9	100
Cr	12.7	11.6	13.5	13.1	13.2	13.5	13.5	13.3	10.9	15.7	16.5	17.2	31.4	32.6	1.4	1.02
Co	33.1	30.7	33.7	34.5	34.9	35.2	34.7	35.5	25.4	34.7	34.2	35.6	28	26.3	9.58	11.8
Ni	14.9	13	16	16.5	17.1	17.3	16.6	18	7.18	9.99	9.79	10.3	20.2	17.7	2.35	2.63
Cu	224	203	227	220	223	240	226	238	127	184	169	179	191	187	117	143
Zn	107	136	116	120	114	116	115	116	86.6	111	112	114	100	96.9	70.3	74.2
As	25.1	6.22	6.78	3.1	7.12	10.5	6.82	8.08	3.19	4.37	4.68	4.61	5.37	5.99	4.38	3.9
Rb	43.9	42.3	49.9	51.4	49.2	51.5	49.3	50.1	25.8	32.9	34.7	34	37.2	38.3	169	130
Sr	475	478	470	457	459	461	453	457	558	497	457	473	483	489	1870	1170
Y	26	26	28	27.5	27.2	27.6	27.3	27.4	18.9	23.3	23.5	24	21	22.2	15.5	17
Zr	110	108	116	115	114	116	114	115	55.7	75	76.2	77	65.7	68.5	106	118
Nb	5.97	5.83	6.18	6.25	6.11	6.26	6.19	6.16	2.63	3.03	3.07	3.06	3.05	3.16	4.86	5.54
Cd	0.0498	0.108	0.0574	0.0541	0.0487	0.0538	0.055	0.058	0.0441	0.0513	0.0469	0.0488	0.045	0.0461	0.0391	0.049
Cs	1.51	1.73	1.86	1.97	1.76	1.96	1.84	2	0.884	1.12	1.23	1.19	1.35	1.59	3	1.11
Ba	967	948	1030	990	1030	1010	1000	1010	607	842	823	847	717	742	1350	1250
La	10.5	10.5	11.2	11.2	11.1	11.3	11.2	11.2	5.7	7.46	7.54	7.62	7.14	7.39	19.7	21.4
Ce	22.7	22.6	23.9	24.3	23.8	24	23.9	23.9	12.4	16.2	16.4	16.5	15.4	15.7	36.5	39.9
Pr	3.21	3.21	3.42	3.46	3.36	3.42	3.41	3.41	1.83	2.39	2.41	2.42	2.22	2.29	4.69	5.13
Nd	14.7	14.6	15.5	15.8	15.5	15.7	15.4	15.4	8.64	11.3	11.5	11.7	10.3	10.7	18.4	20.2
Sm	3.87	3.94	4.24	4.29	4.16	4.2	4.25	4.18	2.48	3.24	3.33	3.37	2.81	2.92	3.74	4.13
Eu	1.21	1.23	1.27	1.27	1.26	1.28	1.28	1.24	0.858	1.09	1.07	1.1	0.98	1.04	1.2	1.29
Gd	4.53	4.46	4.74	4.71	4.73	4.67	4.66	4.73	2.96	3.87	3.92	3.96	3.34	3.52	3.3	3.59
Tb	0.713	0.717	0.747	0.758	0.745	0.754	0.755	0.753	0.479	0.623	0.645	0.66	0.542	0.58	0.456	0.487
Dy	4.5	4.55	4.65	4.77	4.68	4.85	4.78	4.78	3.19	4.08	4.18	4.23	3.58	3.77	2.54	2.84
Ho	0.925	0.929	1	1.01	0.984	0.986	0.975	0.984	0.665	0.844	0.869	0.868	0.746	0.789	0.503	0.548
Er	2.75	2.65	2.84	2.89	2.84	2.89	2.86	2.87	1.99	2.48	2.53	2.57	2.23	2.32	1.44	1.62
Tm																
Yb	2.53	2.55	2.64	2.71	2.64	2.69	2.65	2.67	1.87	2.32	2.36	2.4	2.13	2.18	1.39	1.59
Lu	0.375	0.368	0.397	0.403	0.394	0.398	0.394	0.395	0.271	0.331	0.347	0.349	0.313	0.329	0.211	0.239
Hf	2.99	2.92	3.17	3.18	3.15	3.15	3.1	3.12	1.61	2.18	2.25	2.27	1.81	1.87	2.55	2.81
Ta	0.368	0.37	0.39	0.39	0.388	0.392	0.385	0.384	0.166	0.191	0.189	0.194	0.192	0.193	0.282	0.303
Tl	0.298	0.234	0.322	0.36	0.361	0.297	0.245	0.272	0.2	0.268	0.317	0.222	0.282	0.297	0.351	0.138
Pb	9.64	9.7	10.2	10.5	10.1	10.2	10.2	10.1	6	9.58	9.9	9.67	4.63	4.74	10.9	12.1
Th	1.98	1.97	2.07	2.11	2.06	2.1	2.08	2.09	1.03	1.39	1.4	1.41	1.19	1.23	4.46	4.95
U	1.08	1.08	1.18	1.11	1.12	1.11	1.1	1.11	0.517	0.854	0.857	0.843	0.528	0.532	1.22	2.19

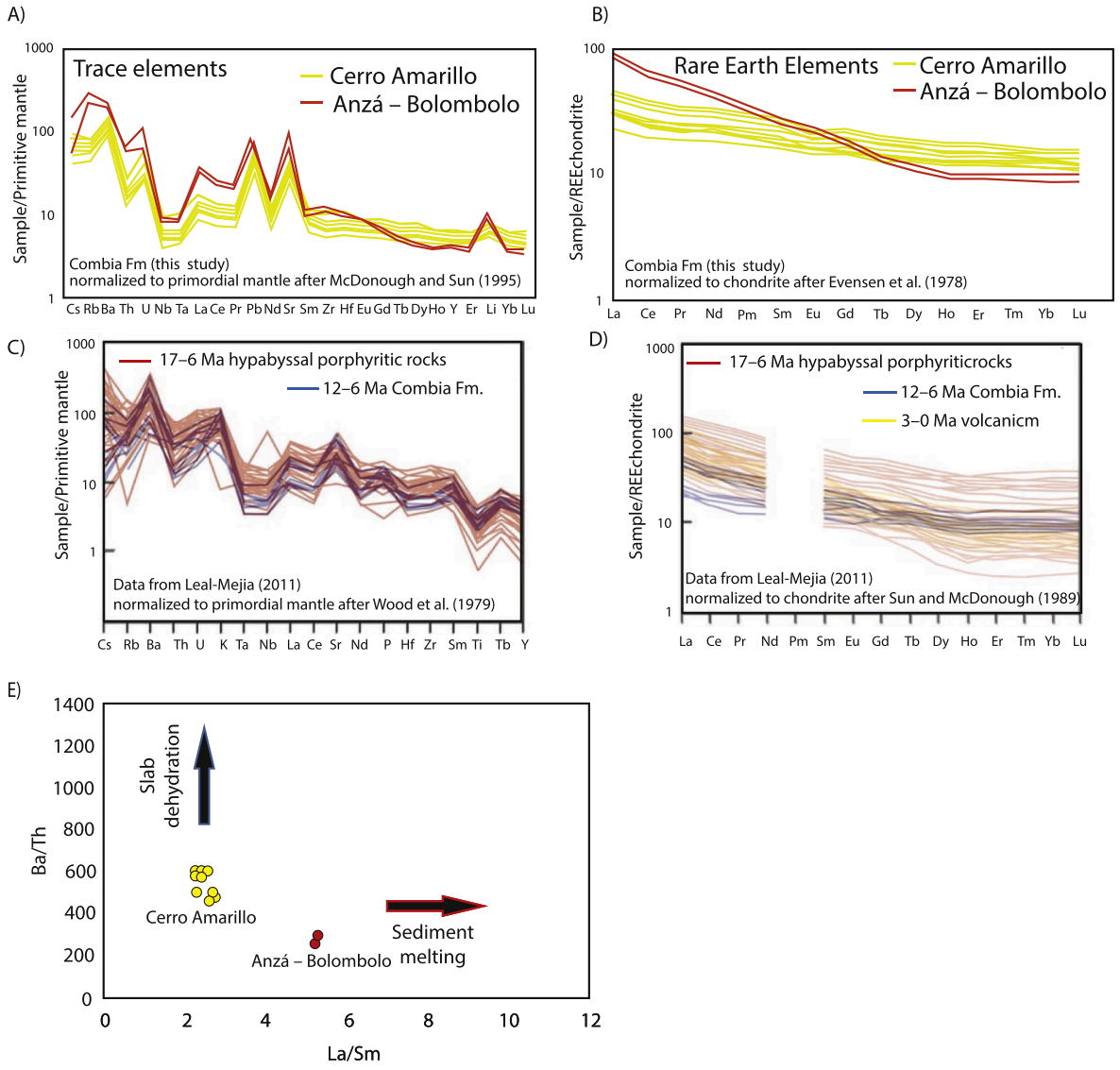

Fig. 9. A) Primordial mantle (McDonough and Sun, 1995) normalized trace element spider diagrams of volcanic rocks from the Cerro Amarillo and Anzá-Bolombolo sections. B) Chondrite normalized (Evensen et al., 1978) Rare Earth Element (REE) patterns of the volcanic rocks from the Cerro Amarillo section. C) For comparison trace element patterns of published data by Leal-Mejia (2011) from Combia Formation and hypabyssal porphyritic intrusions in the study area, as summarized in Marín-Cerón et al. (2019). Trace element data normalized after Wood et al. (1979). D) For comparison, published REE data of Leal-Mejía (2011) normalized after Sun and McDonough (1989) for hypabyssal porphyritic intrusions, Combia Formation volcanic rocks and recent to present volcanism in the Central Cordillera, as summarized in Marín-Cerón et al. (2019). E) The La/Sm versus Ba/Th plot indicates that the Cerro Amarillo volcanic rocks were more derived from magma related to slab dehydration, whereas the Anzá-Bolombolo samples trend more towards sediment melting derived magma.

Table 6
Isotopic compositions of volcanic rocks from the Cerro Amarillo and Anzó Bolombolo sections.

	JJ1-3	JJ1-9	JJ1-17	JJ1-23	JJ3-2	JJ3-5	JJ3-9	JJ4-2	JJ2-1-10	JJ2-1-14
$^{87}Sr/^{86}Sr$	0.703911	0.703930	0.703931	0.703921	0.703916	0.703876	0.70387	0.703862	0.70417	0.70416
2σ	0.000006	0.000008	0.000008	0.000008	0.000006	0.000006	0.000006	0.000006	0.000006	0.000006
$^{87}Sr/^{86}Sr$ (leached)	0.70391	0.70393	0.70393	0.70393	0.70392	0.70388	0.70387	0.70387	0.70417	0.70417
2σ	0.000006	0.000006	0.000006	0.000008	0.000006	0.000006	0.000006	0.000006	0.000006	0.000006
$^{143}Nd/^{144}Nd$	0.51294	0.51293	0.51292	0.51295	0.51293	0.51296	0.51293	0.51298	0.51290	0.51289
2σ	0.000009	0.000018	0.000017	0.000010	0.000010	0.000007	0.000013	0.000008	0.000007	0.000010
εNd	5.959	5.930	5.684	6.223	5.846	6.420	5.905	6.882	5.255	5.191
$^{208}Pb/^{204}Pb$	38.72422	38.73927	38.73610	38.73702	38.71385	38.67951	38.68273	38.79674	38.74386	38.75921
2σ	0.00418	0.00418	0.00418	0.00418	0.00418	0.00417	0.00417	0.00418	0.004179	0.004180
$^{207}Pb/^{204}Pb$	15.61989	15.62459	15.62410	15.62365	15.62449	15.61989	15.62098	15.61286	15.60328	15.61037
2σ	0.00167	0.00167	0.00167	0.00167	0.00167	0.00167	0.00167	0.00167	0.001668	0.001669
$^{206}Pb/^{204}Pb$	18.96667	18.97333	18.97308	18.97264	18.93568	18.91002	18.91054	19.06522	19.00789	19.018005
2σ	0.00365	0.00365	0.00365	0.00365	0.00365	0.00364	0.00364	0.00367	0.003662	0.003666

Table 7
Estimated isotopic compositions and parameters for end-member involved in magma genesis.

	$^{208}Pb/^{204}Pb$	$^{206}Pb/^{204}Pb$	Pb (ppm)	$^{142}Nd/^{144}Nd$	Nd (ppm)	$^{87}Sr/^{86}Sr$	Sr (ppm)
AOC[1,9]	38.14	18.59	0.53	0.51280	4.71	0.70381	61.40
HS[2,3,4]	38.86	18.64	9.59	0.51247	17.0	0.70763	336.16
CS[2,3,4,5]	38.16	18.46	3.70	0.51242	0.89	0.70858	1504.12
SC_1[a]	38.62	18.62	1.43	0.51285	5.94	0.70454	75.138
SC_2[a]	38.57	18.60	1.54	0.51284	1.15	0.70661	146.412
MW[6,7]	37.90	18.50	0.02	0.51310	0.71	0.70270	9.80
PM[a]	38.45	18.59	0.82	0.51307	5.81	0.70469	114.95
LCC[8]	38.73	19.02	8.81	0.51309	9.50	0.70423	173.00

[a] Estimated values. Kd from Halliday et al. (1995). AOC: Altered oceanic crust; HS: Hemipelagic sediments; CS: Carbonaceous sediments; SC_1: Subduction component 1 (AOC + HS); SC_2: Subduction component 2 (SC_1 + CS); MW: Mantle wedge (5%cpx, 25%opx, 70%ol); PM: Primary magma; and LCC: Lower continental crust. Values are calculated based on procedures followed by Marín-Cerón (2007) for the SW Colombian volcanic arc. Values for AOC, HS, CS, MW, and LCC, are given according to data presented by Marín-Cerón (2007). SC_2 represents the interaction between AOC (85%) and sediments (HS – 10% and CS – 5%). PM is calculated assuming 40% of metasomatized mantle by subduction component. It is considered 10% of LCC interacts with primary magma for magma source genesis.[1]Pedersen et al. (2001); [2]Plank and Langmuir (2000);[3]Patiño et al. (2000); [4]Vervoort et al. (1999);[5]Hemming and McLennan (2001); [6]Salters and Stracke (2004);[7]Saunders et al. (1988);[8]Weber et al. (2002);[9]Barret (1983); and[10]Halliday et al. (1995).

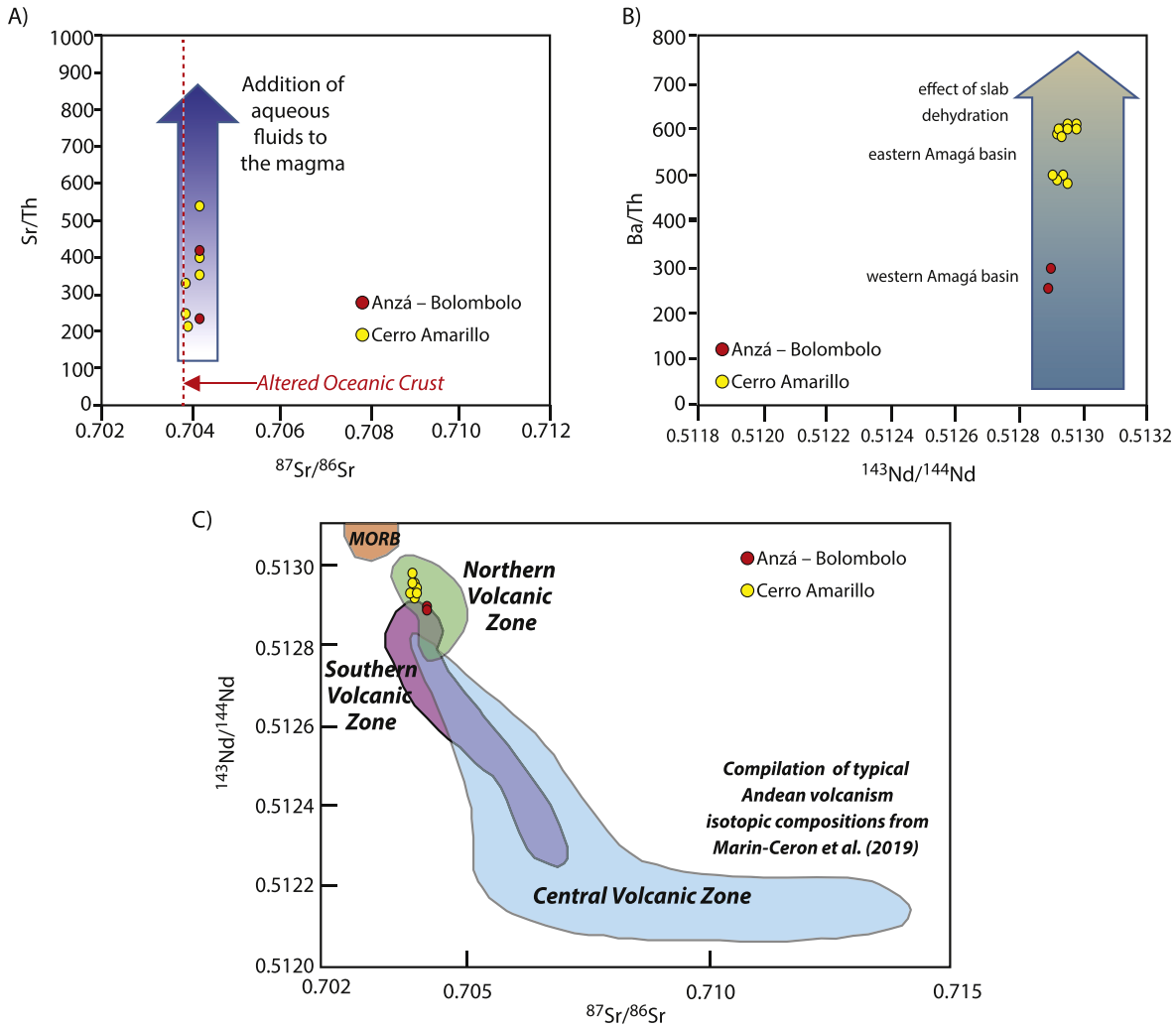

Fig. 10. Comparison between trace elements and isotopic systematics: A) Sr/Th versus $^{87}Sr/^{86}Sr$, and B) Ba/Th versus $^{143}Nd/^{144}Nd$, for volcanic rocks of the CA section (blue circles) and the AB section (red circles). The dashed line represents altered oceanic crust values (AOC) (after Barret, 1983). Both diagrams show that addition of fluids to the magma affected the geochemistry to the analyzed rocks and that the slab dehydration effects are more pronounced in the eastern than the western Amagá basin. C) Nd vs. Sr isotope ratio plot, showing the fields for the Northern Volcanic Zone (NVZ), Central Volcanic Zone (CVZ) and Southern Volcanic Zone (SVZ) as well as typical MORB composition, based on data from James et al. (1976); Hawkesworth et al. (1979); James (1982); Harmon et al. (1984); Frey et al. (1984); Thorpe (1984); Hickey et al. (1986); Hildreth and Moorbath (1988); Wörner et al. (1988); Walker et al. (1991); de Silva (1991); Kay et al. (1991); Davidson and de Silva (1992). Winter (2001); Marín-Cerón (2007), as summarized by and plot modified from Marín-Cerón et al. (2019). The data of our study are shown for the Cerro Amarillo section (yellow circles) and the Anzá-Bolombolo section (red circles), plotted over the NVZ field. (For interpretation of the references to color in this figure legend, the reader is referred to the Web version of this article.)

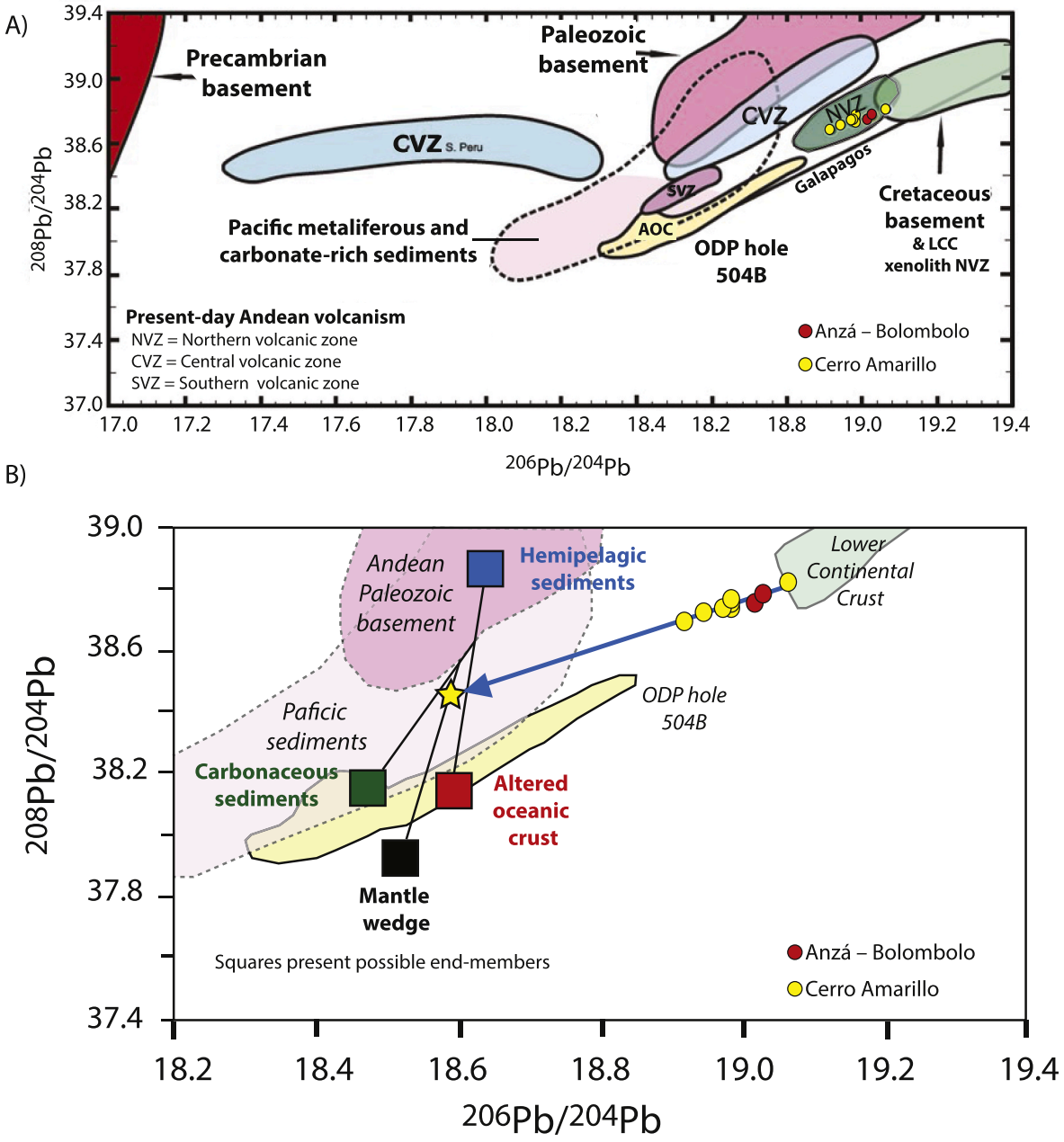

Fig. 11. Lead isotopic systematics of the Combia Formation shown for the Cerro Amarillo section (yellow circles) and the Anzá-Bolombolo section (red circles). A) Plots of $^{208}Pb/^{204}Pb$ vs $^{206}Pb/^{204}Pb$ for the Andean volcanic zones (Northern Volcanic Zone – NVZ; Central Volcanic Zone – CVZ; and Southern Volcanic Zone – SVZ) and the pre-Andean basement (plot modified from data compilation plot of Marín-Cerón (2019). Pacific sediments (Dasch, 1981; White et al., 1985); Paleozoic basement (Chiaradia and Fontboté, 2002); metalliferous sediments from DSDP leg 92 (Barret et al., 1987). B) Zoom on the $^{208}Pb/^{204}Pb$ vs $^{206}Pb/^{204}Pb$ diagram. Squares represent possible end-members and the respective trends of the interaction between each of the components involved during magma formation. AOC: altered oceanic crust; HS: hemipelagic sediments; CS: carbonaceous sediments; LCC: lower continental crust. The solid blue line represents the linear trend of the samples suggesting bimodal mixing between primary magma (yellow star) and LCC. This plot is based on the compilation of Marín-Cerón et al. (2019); Cretaceous Domain (Kerr, 2003); Lower crust xenotiths (Weber et al., 2002); and ACC from Hole 504 (Pedersen and Furnes, 2001); NVZ data from Marín-Cerón (2007). The data from our study are shown for the Cerro Amarillo section (yellow circles) and the Anzá-Bolombolo section (red circles) and the plotted over the Northern Volcanic Zone field. (For interpretation of the references to color in this figure legend, the reader is referred to the Web version of this article.)

spherulitic textures, embayments, reaction rims, coronas and crystal zoning. These textures are attributed to different conditions and magmatic processes such as pressure variations, zoned magma chambers, decompression, magma mixing, phenocrysts recycling and fractional crystallization (e.g. Nixon and Pearce, 1987; Nelson and Montana, 1992; Singer et al., 1995; Perugini et al., 2003; Aldanmaz, 2006; Maro and Remesal, 2011). Thus, our petrographic results favor mainly magma mixing and fractional crystallization to be the main causes for disequilibrium in the magma chamber. as it is supported by the geochemical modelling explained below.

5.3. Magma genesis

Magmatic arcs are the result of subduction of oceanic crust beneath continental crust and this complex setting has impact on magmatic processes such as partial melting, fractional crystallization, changes in

pressure and temperature, sediment melting, dehydration, and decarbonation (e.g. Rollinson, 1993; Albarade, 1995; White, 2013). In addition, fluids added to the mantle wedge play an important role, as fluids allow the transport of incompatible elements from the subducted oceanic basalt and sediments to the magma, leading to enrichment in specific mobile elements and modifying the isotopic composition of the asthenospheric magma source (Tatsumi, 2005; Tatsumi and Stern, 2006; Tatsumi and Takahashi, 2006; Nakamura et al., 1985).

As we have discussed before, we correlate the Cerro Amalillo basaltic lava and the basaltic pyroclastic flows, with the 12-9 Ma event proposed by Bissig et al. (2017) for the Middle Cauca Metalogenic Belt. Our new geochemical data for the Cerro Amarillo area are generally similar to what was previously published by Marriner and Millward (1984) and by Ordoñez (2002), as shown in Fig. 7B. Major elements allow identification of a tholeiitic trend in the samples from the eastern Amagá basin while the samples from the western Amagá basin follow a calc-alkaline trend (Fig. 7A). Both magma suites have been previously recognized at other sampling sites of the Combia Formation (Fig. 7A; e.g. Álvarez, 1983; Marriner and Millward, 1984; Ordoñez, 2002; Leal-Mejía, 2011). With SiO_2 contents between 47 and 54 wt% our Cerro Amarillo samples plot in the basaltic andesite field of Fig. 7B. Additionally, as proposed by Bissig et al. (2017) for the Middle Cauca Metalogenic Bel and given our thermochronological data, we correlate the samples from the Anzá Bolombolo section and the upper portion of the La Metida Creek seek section with the <9-6 Ma Combia event. The samples from Anzá Bolombolo plot in the trachy-andesite field of LeMaitre et al. (1989) and Cox et al. (1979) (Fig. 7B). For comparison, published data for the Combia Formation are also shown in this figure. It appears that the Anzá-Bolombolo section samples from the western Amagá basin are much more alkaline than others (Fig. 7B), and that samples from both sections have lower SiO_2 contents than the volcanic rocks of the 24-20 Ma magmatic phase and most of the 17-9 Ma magmatic phase rocks analyzed by Leal-Mejía (2011). Despite these differences, no precise division of the basin with respect to the magmatic suites can so far be given, and more detailed mapping and geochemical analyses are necessary.

The trace elements provide clear evidence of a subduction-related geochemical signature, with Nb and Ta depletion (e.g. Wilson, 1989; White, 2013). Samples also all have very high Ba, U, Pb and Sr contents, as already noticed for previously published Combia Formation data (Fig. 9C and D, Leal-Mejía, 2011; data summarized in Marín-Cerón et al., 2019). Medium to slightly elevated Ba/Th values, a proxy for slab dehydration characterize the Cerro Amarillo samples from the eastern Amagá basin (Fig. 9E; Labanieh et al., 2012), whereas the Anzá-Bolombolo samples of the western Amagá basin have low ratio, more consistent with a sediment melting trend (Fig. 9E).

In general, the trace element results of the Amagá basin resemble those of the NVZ of the Andes, as summarized in Ancellin et al. (2017); Marín-Cerón et al. (2019), even though the Combia Formation has higher LILE (Rb, Sr, Ba) contents and lower Nb and Ta contents than those reported for the NVZ (Thorpe et al., 1982; Marriner and Millward, 1984).

The REE patterns of samples from the Anzá Bolombolo and Cerro Amarillo sections are somewhat different, with higher fractionation in the former group (Fig. 9b). In comparison to the REE spectra of the 9-6 Ma porphyritic intrusions and recent volcanism, the Combia Formation shows a pattern closer to the latest stage of volcanic activity (Fig. 9D; data from Leal-Mejía (2011), summarized by Marín-Cerón et al. (2019)). The difference in the slope of the REE patterns of eastern (Cerro Amarillo) and western (Anzá Bolombolo) Amagá basin samples suggest differences in terms of magma formation, most probably during melting processes in the mantle source, and/or amphibole fractionation in the crust. Overall, the absence of an Eu anomaly suggests that melting occurred relatively deep, below the plagioclase stability level (~40 km depth).

Combining trace element data with isotopic data can help understanding the origin of magmas and the potential role of subducted slab addition to the mantle wedge (e.g. Tatsumi, 2005; Tatsumi and Stern, 2006). The Cerro Amarillo and Anzá-Bolombolo samples have medium to slightly elevated Sr/Th and rather low $^{87}Sr/^{86}Sr$ ratios (Fig. 10A), indicating transfer of elements from the subducted slab by NVZ aqueous fluids. Because no systematic difference in $^{87}Sr/^{86}Sr$ is observed between leached and unleached samples (Table 6), post-emplacement alteration can be excluded, and the measured ratios can be considered as representative of the magma source (e.g. Tamura and Nakamura, 1996; Shibata and Nakamura, 1997). Similarly, the large range of Ba/Th values at almost constant $^{143}Nd/^{144}Nd$ values indicates addition of Ba through slab dehydration (Fig. 10B), with a stronger effect in the eastern Amagá basin than in the western part of the basin. In an $^{87}Sr/^{86}Sr$ vs $^{143}Nd/^{144}Nd$ isotopic space (Fig. 10C), the Amagá basin samples fall as expected within the field defined by the NVZ (see compilation of Ancellin et al., 2017; Marín-Cerón et al., 2019). The Anzá-Bolombolo samples have slightly more enriched isotopic characteristics than the Cerro Amarillo samples, a feature consistent with the difference seen in Fig. 9E since sediment addition tends to lower the Nd isotopic composition and increase the Sr isotopes.

Lead isotopes provide complementary and useful information. As was the case for Sr and Nd isotopic data, the Amagá basin samples fall in the field defined by the NVZ and differ drastically from fields defined by the CVZ and SVZ (Fig. 11A) (see compilations made by Marín-Cerón, 2007 and Marín-Cerón et al., 2010, 2019). The rather radiogenic values of Pb isotopes for the NVZ have been interpreted as being due either to an enriched mantle reservoir or to continental crust assimilation. The enriched mantle hypothesis was suggested by Rodríguez-Vargas et al. (2005) on the basis of the Nd and Sr isotopic characteristics of xenoliths from the Mercaderes region in SW Colombia. The authors invoked the potential involvement of magma material coming from the Galapagos plume, but such influence under the Amagá basin seems quite unlikely given the distance between the SW Colombian arc and the Galapagos (>450 km, Pedersen and Furnes, 2001). However, the Amagá Basin samples analyzed in this study provide new information because they define a tight correlation in $^{208}Pb/^{204}Pb$ vs $^{206}Pb/^{204}Pb$ space (see Fig. 11B). Such linear array implies the involvement and mixture of two endmembers whose compositions remain unchanged during the entire volcanic sequence. The enriched end-member seems to correspond to the local lower continental crust (Weber et al., 2002; see Fig. 11B), whereas the less radiogenic endmember is more ambiguous. Following the Marin-Ceron et al. (2019) model, this 'depleted' endmember could correspond to the mantle wedge whose composition would be affected by the presence of material originating from the subducted slab (see Fig. 11B). Nonetheless, there may be differences in the subduction mechanisms, proportion of end-members interaction, and magma source evolution between magmatism at 12-9 and 9-6 Ma, and magmatism at 3 Ma – present, despite assuming the same end-members.

In summary, magma was generated by slab dehydration, sediment melting and interactions with the LCC, resulting in the mixing of at least two end-member sources. Due to differences in depth of melting and other magmatic processes (assimilation-fractional crystallization (AFC) and melting-assimilation-storage-homogenization (MASH)), as shown in Fig. 12, the late Miocene volcanic rocks of the western Amagá Basin such as the Anzá Bolombolo and the upper La Metida Creek sections (correlate with the <9-6Ma event) and the eastern Amagá basin such as the Cerro Amarillo section (correlate with the 12-9 Ma event), show distinct petrologic and geochemical signatures.

The geochemical modeling of trace element and Nd, Sr and Pb isotopic data indicates a complex magmatic process including slab dehydration and/or sediment melting, which produces metasomatism of the mantle wedge allowing the formation of a primary magma with different degrees of partial melting. Then, the hot-zone developed a high Pb-radiogenic, garnet-bearing lower continental crustal (LCC) level as a consequence of the quantity of dehydration and of changes of the tectonic regime style. An extensional pull-apart event (12- 9 Ma), may have

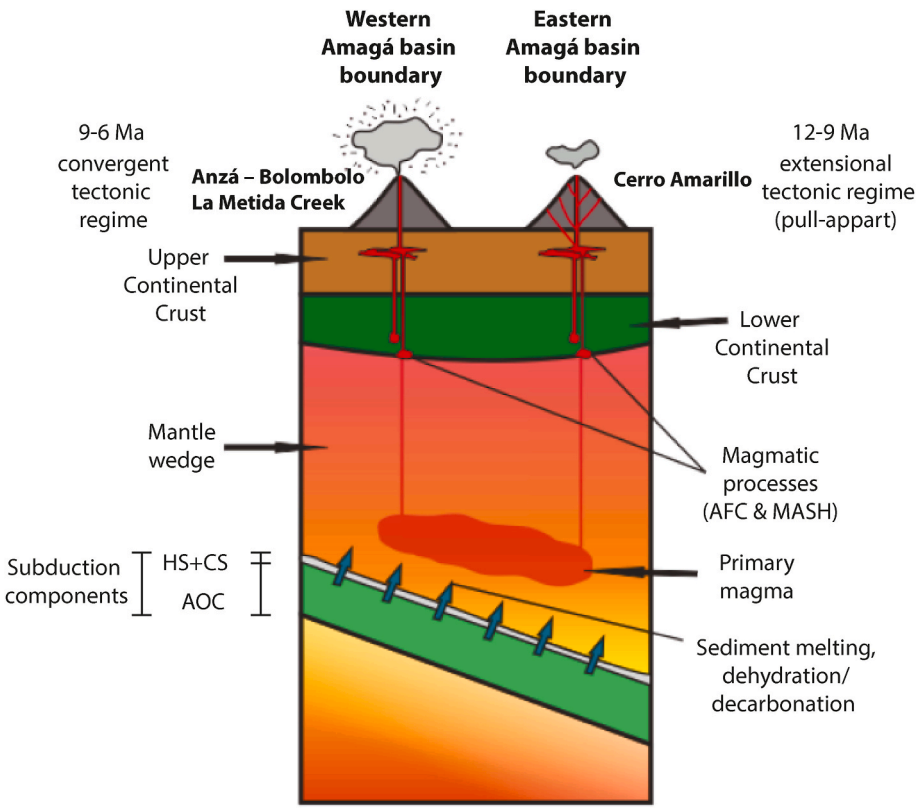

Fig. 12. Schematic diagram for magma source genesis of Combia Formation volcanism. AOC: altered oceanic crust; HS: hemipelagic sediments; CS: carbonaceous sediments; AFC: assimilation fraction crystallization processes (DePaolo, 1981); MASH: melting, assimilation, storage, and homogenization processes (Hildreth and Moorbath, 1988); LCC: lower continental crust; UCC: upper continental crust. Illustration based on model proposed for southwestern Colombian volcanism (Marín-Cerón, 2007) and is compatible with models presented in Marín-Cerón et al. (2019).

facilitated rapid magma ascends to the uppermost crust along a subvertical magma plumbing system throughout the Romeral Fault zone (e.g. permineralized stage from Bissig et al., 2017). Furthermore, the calc-alkaline magmas that have adakite-like signatures, may indicate convergent tectonics that allowed the formation of middle-to upper--crustal magma chambers with garnet fractionation at depth and the evolution of silicate melts into the hot zone mainly related to the amount of water present (>4 wt %) at 9-6 Ma. A new period of extensional pull-apart events started at 6-3 Ma (e.g. Irra basin, Sierra et al., 2012).

Using these results, we propose a model where the differences in the crustal thickness may not be the main driver for the formation of the late Miocene-Pliocene magmatism in the Amaga basin, but may correlate with the extensional to compressional regime (e.g. Sierra et al., 2012; Bissig et al., 2017). Thus, the changes of the late Miocene magmatism are mainly related to the mantle-derived magmas metasomatized by the slab components, and the interaction with the high-Pb radiogenic LCC, where the stability of garnet may play the most important role in the geochemistry of the magmas and their fertility as proposed by Bissig et al. (2017).

6. Conclusions

The late Miocene volcanic and volcanoclastic Combia Formation of the Amagá basin between in the Central and Western Cordillera developed above the Nazca plate subduction zone in western Colombia. Volcanic and volcaniclastic rocks of the Combia Formation are characterized by a sequence of ignimbrites and lava flows of tholeiitic affinity at the bottom and pyroclastic flows to the top of the formation in the eastern Amaga basin and a succession of pyroclastic and epiclastic flows with calc-alkaline affinity in the western Amagá basin. Using apatite and zircon fission-track dating the timing of volcanic activity during the deposition of the Combia Formation was confirmed between 12 and 6 Ma.

Trace element, REE and Nd, Sr and Pb isotopic analyses show that the surface weathering did not modify the geochemical signatures and that the geochemical composition of the samples results of several magmatic processes including oceanic crusts (AOC), slab includes AOC and sediment dehydration and melting. As the subduction components metasomatize the mantle wedge, primary magmas are produced. Then, the hot-zone developed a high Pb-radiogenic, garnet-bearing lower continental crustal level as a consequence of the quantity of dehydration and of the changes of the tectonic regime. An extensional pull-apart event (e.g at ca. 12-9 Ma, Cerro Amarillo section), most likely facilitated rapid magma ascend to the uppermost crust along a subvertical magma plumbing system throughout the Romeral Fault zone.

In contrast, Calc-alkaline magmas with adakite-like signatures of the Anzá Bolombolo and the upper La Metida Creek sections may indicate convergent tectonics that allowed the formation of middle-to upper-crustal magma chambers with a garnet fractionation at depth and the evolution of silicate melts in the hot zone, mainly related to the amount of water (>4 wt %) present at 9-6 Ma to form the primary magmas in the mantle wedge and mixing of this primary magma with lower continental crustal before eruption. In contrast, contamination by upper crustal rocks could not be detected. Finally, the new geochemical results confirm that Combia Formation volcanism in the Amagá basin between 12 and 6 Ma was similar to what is known about the NVZ of the Andes in South America, related to Nazca plate subduction, and with periods of extension (12-9 Ma; 6-3 Ma) and contraction (<9-6 Ma; 3 Ma-Present).

Author contribution

All authors contributed to the writing of the manuscript. Matthias Bernet complied the first draft, facilitated and oversaw the thermochronological analyses and obtained funding for the project. Juliana Mesa-Garcia did the field work and sample analysis (thermochronology, petrology and geochemistry). Maria Jackeline Ramirez did part of the field work and sample analysis (petrology). Catherine Chauvel facilitated and oversaw the geochemical analyses. Maria Isabel Marin Ceron

developed the study and managed the interactions with the ANH and obtained funding for the project.

Declaration of competing interest

The authors declare that they have no known competing financial interests or personal relationships that could have appeared to influence the work reported in this paper.

Acknowledgements

We acknowledge support of this study from ECOS-NORD (France) and Colciencias/ ICETEX (Colombia) project C12U01 of M. Bernet and M.I. Marín-Cerón, as well as a BQR SUD grant at ISTerre, awarded to M. Bernet. We thank Wilton Echavarría, Francois Senebier and Francis Coeur for help with sample preparation and mineral separation.

Appendix A. Supplementary data

Supplementary data to this article can be found online at https://doi.org/10.1016/j.jsames.2020.102897.

Note – RhoS: spontaneous track density. RhoI: induced track density; P (χ^2): Chi^2 probability. Fission-track ages were calculated using a Zeta value of 191.6 ± 10.25. ZFT data calculated with Binomfit of Brandon (see Ehlers et al., 2005).

References

Albarade, F., 1995. Introduction to Geochemical Modelling. Cambridge University Press, p. 543 pp.
Aldanmaz, E., 2006. Mineral – chemical constraints in the Miocene calc-alkaline and shoshonitic volcanic rocks of Western Turkey: disequilibrium phenochryst assemblages as indicators of magma storage and mixing conditions. Turk. J. Earth Sci. 15, 47–73.
Álvarez, A., 1983. Geología de la cordillera Central y el Occidente colombiano y petroquímica de los intrusivos granitoides Mesocenozoicos. Bol. Geol. 26, 175 pp..
Ancellin, M.A., Samaniego, P., Vlastelic, I., Nauret, F., Gannoun, A., Hidalgo, S., 2017. Across-arc versus along-arc Sr-Nd-Pb isotope variations in the Ecuadorian volcanic arc. G-cubed 18, 1163–1188. https://doi.org/10.1002/2016GC006679.
Aspden, J.A., McCourt, W.J., Brook, M., 1987. Geometrical Control of Subduction-Related Magmatism: the Mesozoic and Cenozoic Plutonic History of Western Colombia, vol. 144. Journal of the Geological Society, London, pp. 893–905.
Barret, T.J., 1983. Strontium- and lead-isotope composition of some basalts form deep sea drilling project Hole 504B, Costa Rica rift, legs 69 and 70. In: Cann, J.R., Langseth, M.G., Honnorez, J., VonHerzen, R.P., White, S.M., et al. (Eds.), Init. Repts. DSDP, vol. 69. U.S. Govt. Printing Office, Washington, pp. 643–650.
Barret, T.J., Taylor, P.N., Lugowski, J., 1987. Metalliferous sediments from DSDP leg 92: the east pacific rise transects. Geochem. Cosmochim. Acta 46, 651–666.
Bernet, M., Uruena, C., Amaya, S., Pena, M.L., 2016. New thermo- and geochronological constraints on the Pliocene-Pleistocene eruption history of the Paipa-Iza volcanic complex, Eastern Cordillera, Colombia. J. Volcanol. Geoth. Res. 327, 299–309.
Bissig, T., Leal-Mejía, H., Stevens, R., Hart, C., 2017. High Sr/Y magma petrogenesis and the link to porphyry mineralization as revealed by garnet-bearing I-type granodiorite porphyries of the middle Cauca Au-Cu belt, Colombia. Society of economic geologists, inc. Economic Geology, 112, pp. 551–568.
Blandon, A., Parra, N., Gorin, G.E., Arango, F., 2008. Adapting palynological preparation methods in subbituminous and bituminous coals from Colombia to improve palynofacies and hydrocarbon source rock evaluations. Int. J. Coal Geol. 73, 99–114.
Calle, B., González, H., 1980. Geología y geoquímica de la Plancha 166, jericó. Informe no. 1822. Medellín. INGEOMINAS, p. 232.
Cediel, F., Shaw, R.P., Caceres, C., 2003. Tectonic assembly of the northern andean block. In: Bartolini, C., Buffler, R.T., Blickwede, J. (Eds.), The Circum-Gulf of Mexico and the Caribbean: Hydrocarbon Habitats, Basin Formation, and Plate tectonics.-AAPG Memoir, vol. 79, pp. 815–848.
Cediel, F., Leal-Mejía, H., Shaw, R.P., Melgarego, J.C., Restrepo-Pace, P.A., 2011. Petroleum Geology of Colombia: regional Geology of Colombia. ANH – Colombia 1, 220 pp..
Chauvel, C., Bureau, S., Poggi, C., 2011. Comprehensive chemical and isotopic analyses of basalt and sediment reference materials. Geostand. Geoanal. Res. 35 (1), 125–143.
Chiaradia, M., Fontbote, L., 2002. Lead isotope systematics of Late Cretaceous Tertiary Andean arc magmas and associated ores between 8°N and 40°S: evidence for latitudinal mantle heterogeneity beneath the Andes. Terra. Nova 14 (5), 337–342.
Cox, K.G., Bell, J.D., Pankhurst, R.J., 1979. The Interpretation of Igneous Rocks. George Allen & Unwin, London, p. 464 pp..
Dasch, E.J., 1981. Lead isotopic composition of metalliferous sediments from the Nazca Plate. Mem. Geol. Soc. Am. 154, 199–209.
Davidson, J.P., de Silva, S.L., 1992. Volcanic rocks from the Bolivian Altiplano: insights into crustal structure, contamination, and magma genesis in the central Andes. Geology 20, 1127–1130.
de Silva, S., 1991. Styles of zoning in Central Andean ignimbrites-insights into magma chamber processes: in: Andean magmatism and its tectonic setting. Special paper 265, 217–232.
DePaolo, D.J., 1981. Trace-element and isotopic effects of combined wallrock assimilation and fractional crystallisation. Earth Planet Sci. Lett. 53, 189–202.
Ehlers, E.G., 1987. Optical Mineralogy, vol. 2. Mineral Descriptions. Blackwell Scientific Pub, Palo Alto.
Ehlers, T.A., Chaudhri, T., Kumar, S., Fuller, C., Willett, S.D., Ketcham, R., Brandon, M. T., 2005. Computational tools for low-temperature thermochronometer interpretation. In: Reiners, P.W., Ehlers, T.A. (Eds.), Low-temperature Thermochronology. Techniques, Interpretations and Applications. Reviews in Mineralogy and Geochemistry. Mineralogical Society of America, pp. 589–622. https://doi.org/10.2138/rmg.2005.58.22.
Evensen, N.M., Hamilton, P.J., O'Nions, R.K., 1978. Rare-earth abundances in chondritic meteorites. Geochem. Cosmochim. Acta 42, 1199–1212.
Farris, D.W., Jaramillo, C., Bayona, G., Restrepo-Moreno, S.A., Montes, C., Cardona, A., Mora, A., Speakman, R.J., Glascock, M.D., Valencia, V., 2011. Fracturing of the Panamanian isthmus during initial collision with south America. Geology 39 (11), 1007–1010.
Frey, F.A., Gerlach, D.C., Hickey, R.L., López-Escobar, L., Minizaga-Villavicencio, F., 1984. Petrogenesis of the Laguna del Maule volcanic complex, Chile (36°S). Contrib. Mineral. Petrol. 88, 133–149.
González, H., 2001. Memoria Explicativa del Mapa Geológico del Departamento de Antioquia. Escala 1, 400, 000. Medellín, INGEOMINAS. 240 pp.
Grosse, E., 1926. Estudio Geológico del Terciario carbonífero de Antioquia en la parte Occidental de la Cordillera Central de Colombia: Berlín, Verlag Von Dietrich Reimer, p. 361.
Halliday, A.N., Lee, D.-C., Tommasini, S., Davies, G.R., Paslick, C.R., Fitton, J.G., James, D.E., 1995. Incompatible trace elements in OIB and MORB and source enrichment in the sub-oceanic mantle. Earth Planet Sci. Lett. 133, 379–395.
Harmon, R.S., Barreiro, B., Moorbath, S., Hoefs, J., Francis, P.W., Thorpe, R.S., Deruelle, B., McHugh, J., Viglino, J.A., 1984. Regional O-, Sr-, and Pb- isotope relationships in late Cenozoic calc-alkaline lavas of the Andean Cordillera: J. Geol. Soc. 141 (5), 803–822.
Hawkesworth, C.J., Norry, M.J., Roddick, J.C., Baker, P.E., Francis, P.W., Thorpe, R.S., 1979. 143Nd/144Nd, 87Sr/86Sr, and incompatible trace element variations in calc-alkaline andesitic and plateau lavas from South America. Earth Planet Sci. Lett. 42, 45–57.
Hemming, S.R., McLeannan, S.M., 2001. Pb isotopic compositions of modern deep sea turbidites. Earth Planet Sci. Lett. 184, 489–503.
Hickey, R.L., Frey, F.A., Gerlach, D.C., López-Escobar, L., 1986. Multiple sources for basaltic arc rocks from the southern volcanic zone of the Andes (34° - 41° S): trace element and isotopic evidence for contributions from subducted oceanic crust, mantle, and continental crust. J. Geophys. Res. 91 (B6), 5963–5983.
Hildreth, W., Moorbath, S., 1988. Crustal contribution to arc magmatism in the Andes of central Chile. Contrib. Mineral. Petrol. 98, 455–489.
Irvine, T.N., Baragar, W.R.A., 1971. A guide to the chemical classification of the common volcanic rocks: Can. J. Earth Sci. 8 (5), 523–548.
James, D.E., 1982. A combined O, Sr, Nd, and Pb isotopic and trace element study of crustal contamination in central Andean lavas: I. Local geochemical variations. Earth Planet Sci. Lett. 57, 47–62.
James, D.E., Brooks, C., Cuyubamba, A., 1976. Andean Cenozoic volcanism: magma genesis in the light of strontium isotopic composition and trace-element geochemistry. Geol. Soc. Am. Bull. 87, 592–600.
Jaramillo, J.M., 1976. Volcanic Rocks of the Río Cauca Valley, Colombia S.A. Thesis Degree of Master of Arts. Rice University, Houston.
Jaramillo, J.S., Cardona, A., Monsalve, G., Valencia, V., León, S., 2019. Petrogenesis of the lateMiocene Combia volcanic complex, northwestern Colombian Andes: tectonic implication of short term and compositionally heterogeneous arc magmatism. Lithos 330-331, 194–220.
Kay, S., Mpodozis, C., Ramos, V.A., Munizaga, F., 1991. Magma source variations for mid-Tertiary magmatic rocks associated with a shallowing subduction zone and a thickening crust in the Central Andes (28 – 33°S). In: Andean Magmatism and its Tectonic Setting, vol. 265. Colorado, Boulder, pp. 113–137. Harmon, R.S., Rapela, C. W., eds. Spec. Pap. Geol. Soc. Am.
Kellogg, J., Vega, V., 1995. Tectonic Development of Panamá, Costa Rica, and the Colombian Andes: Constraints from Global Positioning System Geodetic Studies and Gravity, vol. 295. Geological Society of America, pp. 75–90.
Kerr, A.C., 2003. Oceanic plateaus. In: Rudnick, R. (Ed.), The Crust., vol. 3 Elsevier Science, Oxford, pp. 537–565. Treatise on Geochemistry.
Kowallis, B.J., Heaton, J.S., Bringhurst, K., 1986. Fission-track dating of volcanically derived sedimentary rocks. Geology 14, 19–22.
Labanieh, S., Chauvel, C., Germa, A., Quidelleur, X., 2012. Martinique: a clear case for sediment melting and slab dehydration as a function of distance to the trench. J. Petrol. 53, 2441–2464.
Leal-Mejía, H., 2011. Phanerozoic Gold Metallogeny in the Colombian Andes – A Tectono-Magmatic Approach: Ph.D. Thesis, Barcelona (Catalonia), Spain. University of Barcelona, p. 1000p.
LeMaitre, R.W., Bateman, P., Dudek, A., Keller, J., Lameyre-LeBas, M.J., Sabine, P.A., Schmid, R., Sorensen, H., Streckeisen, A., Woolley, A.R., Zanettin, B., 1989. Classification of Igneous Rocks and Glossary of Terms. Blackwell, Oxford.

Lesage, G., Richards, J.P., Muehlenbachs, K., Spell, T.L., 2013. Geochronology, geochemistry, and fluid characterization of the late Miocene Buriticá gold deposit, antioquia department, Colombia. Econ. Geol. 108, 1067–1097.
Lonsdale, P., 2005. Creation of the Cocos and Nazca plates by fission of the Farallón plate: Tectonophysics 404 (3 – 4), 237–264.
López, A., Sierra, G.M., Ramírez, S., 2006. Vulcanismo Neógeno en el suroccidente antioqueño y sus implicaciones tectónicas. Boletín Ciencias de la Tierra 19, 27–41.
Mackenzie, W.S., Donaldson, C.H., Guilford, C., 1984. Atlas of Igneous Rocks and Their Textures. Longman Scientific and Technical, UK.
Mantilla, L.C., Bissig, T., Valencia, V., Hart, C.J.R., 2013. The magmatic history of the Vetas–California mining district, santander Massif, eastern cordillera, Colombia. J. S. Am. Earth Sci. 45, 235–249.
Marín-Cerón, M.I., 2007. Major, trace element and multi-isotopic systematics of SW Colombian volcanic arc, northern Andes: contributions of slab fluid, mantle wedge and lower crust to the origin of Quaternary andesites. Doctoral Thesis. Okayama University, Japan.
Marín-Cerón, M.I., Moriguti, T., Makishima, A., Nakamura, E., 2010. Slab decarbonation and CO2 recycling in the Southwestern Colombian volcanic arc. Geochem. Cosmochim. Acta 74, 1104–1121.
Marín-Cerón, M.I., Leal-Mejía, H., Bernet, M., Mesa-Garcia, J., 2019. Late cenozoic to modern-day volcanism in the northern Andes: a geochronological, petrographical, and geochemical review. In: Cediel, F., Shaw, R.P. (Eds.), Geology and Tectonics of Northwestern South America. Frontiers in Earth Sciences, Springer Nature Switzerland, pp. 603–648.
Maro, G., Remesal, M.B., 2011. El vulcanismo de la Alta Sierra de Somún Curá: El Cerro Corona, Provincia de Río Negro. Abstract, Argentina. XVIII Congreso Geológico Argentino. Neuquén. 2 pp.
Marriner, G.F., Millward, D., 1984. Petrochemistry of cretaceous to recent vulcanism in Colombia. Journal of Geological Society of London.141 473–486.
McCourt, W.J., Aspden, J.A., Brook, M., 1984. New Geological and Geochronological Data from the Colombian Andes: Continental Growth by Multiple Accretion, vol. 141. Journal of Geological Society, London, pp. 831–845.
McDonough, W.F., Chauvel, C., 1991. Sample contamination explains the Pb isotopic composition of some Rurutu island and Sasha seamount basalts. Earth Planet Sci. Lett. 105, 397–404.
McDonough, W.F., Sun, S.S., 1995. Composition of the earth. Chem. Geol. 120, 223–253.
Mesa-Garcia, J., 2015. Combia Formation: a Miocene Immature Volcanic Arc? EAFIT University Master thesis, p. 244 pp.
Nakamura, E., Campbell, I.H., Sun, S.S., 1985. The influence of subduction processes on the geochemistry of Japanese alkaline basalt. Nature 316, 55–58.
Nelson, S.T., Montana, A., 1992. Sieve-textured plagioclase in volcanic rocks produced by rapid decompression. Am. Mineral. 77, 1242–1249.
Nixon, G.T., Pearce, T.H., 1987. Laser-interferometry study of oscillatory zoning in plagioclase: the record of magma mixing and phenocryst recycling in calc- alkaline magma chambers, Iztaccihuatl Volcano,. Mexico. Amer. Mineral 72, 1144–1162.
Ordoñez, O., 2002. Caracterizacao Isotopica Rb-Sr E Sm-Nd Dos Principais Eventos Magmáticos Nos Andes Colombianos. Doctoral Thesis. Brazilia University, p. 165 pp..
Páez Acuna, L., 2012. Análisis estratigráfico y de proveniencia del Miembro Superior de la Formación Amagá en los sectores de la Pintada y Valparaiso (cuenca Amagá, andes noroccidentales). Master thesis on Earth Sciences. EAFIT University.
Pardo, N., Cepeda, H., Jaramillo, J.M., 2005. The Paipa volcano, eastern cordillera of Colombia, south America: volcanic stratigraphy. Earth Sci. Res. J. 9, 3–18.
Pardo-Casas, F., Molnar, P., 1987. Relative motion of the Nazca (Farallón) and South American plates since late cretaceous time. Tectonics 6 (3), 223–248.
Patiño, L.C., Carr, M., Feigenson, M., 2000. Local and regional variations in Central American arc lavas controlled by variations in subducted sediment input. Contrib. Mineral. Petrol. 138, 265–283.
Pedersen, R., Furnes, H., 2001. Nd- and Pb-isotopic variations through the upper oceanic crust in DSDP/ODP Hole 504B, Costa Rica Rift. Earth Planet Sci. Lett. 189, 221–235.
Pérez, A.L., 2005. Formación Combia: Litofacies y aproximación a su edad con base en estudios palinológicos, suroeste antioqueño. Undergraduate thesis. EAFIT University, Medellín.
Pérez, A.M., Marín-Cerón, M.I., Bernet, M., Sierra, G., Moreno, N., 2013. Resultados preliminares de AFT en la Formación Amagá, Pozos el Cinco- 1B y Venecia-1. XIV Congreso Colombiano de Geología Libro: XIV Congreso Colombiano de Geología. Resúmenes.
Peccerillo, A., Taylor, S.R., 1976. Geochemistry of Eocene calc-alkaline volcanic rocks from the Kastamonu area, northern Turkey. Contrib. Mineral. Petrol. 58, 63–81.
Perugini, D., Busa, T., Poli, G., Nazzareni, S., 2003. The role of chaotic dynamics and flow fields in the development of disequilibrium textures in volcanic rocks. J. Petrol. 44 (4), 733–756.
Piedrahita, V.A., Bernet, M., Chadima, M., Sierra, G.M., Marín-Cerón, M.I., Toro, G.E., 2017. Detrital zircon fission-track thermochronology and magnetic fabric of the Amagá Formation (Colombia): intracontinental deformation and exhumation events in the northwestern Andes. Sediment. Geol. 356, 26–42.
Ramírez, D.A., López, A., Sierra, G.M., Toro, G.E., 2006. Edad y provenincia de las rocas volcánico sedimentarias de la Formación Combia en el suroccidente Antioqueño-Colombia. Boletin Ciencias de la Tierra 19, 9–26.
Restrepo, J.J., Toussaint, J.F., González, H., 1981. Edades MioPliocenas del magmatismo asociado a la Formación Combia. Departamentos de Antioquia y Caldas, Colombia. Geol. Norandina 3, 2126.
Restrepo-Moreno, S.A., Foster, D.A., Stockli, D.F., Parra-Sánchez, L.N., 2009. Long-term erosion and exhumation of the „altiplano antioqueño", northern Andes (Colombia) from apatite (U-Th)/He thermochronology. Earth Planet Sci. Lett. 278, 1–12.
Restrepo-Moreno, S.A., Cardona, A., Jaramillo, C., Bayona, G., Montes, C., Farris, D.W., 2010. Constraining Cenozoic uplift/exhumation of the Panamá-Chocó Block by apatite and zircon low-temperature thermochronology: insights on the onset of collision and the morphotectonic history of the region. Abstract. GSA Denver Annual Meeting. Geological Society of America Abstracts with Programs 42 (5), 521.
Rios, A.M., Sierra, M.I., 2004. La Formación Combia: Registro de la relación entre el volcanismo Neógeno y la sedimentación fluvial, sección Guineales – Bolombolo, suroeste antioqueño. Undergraduate thesis. EAFIT University, p. 122 pp.
Rodríguez-Vargas, A., Koester, E., Mallmann, G., Conceicao, R.V., Kawashita, K., Weber, M.B.I., 2005. Mantle diversity beneath the Colombian Andes, northern volcanic zone: constraints from Sr and Nd isotope. Lithos 82, 471–484.
Rodríguez, G., Arango, M.I., Bermúdez, J.G., 2012. Batolito de Sabanalarga, plutonismo de arco en la zona de sutura entre las cortezas oceánica y continental de los Andes del Norte. Boletín Ciencias de la Tierra, 32, 81–98.
Rollinson, H.R., 1993. Using Geochemical Data: Evaluation, Presentation, Interpretation. Longman Group UK, p. 352 pp.
Saenz, E.A., 2003. Fission track thermochronology and denudational response to tectonics in the north of the Colombian Central Cordillera. Master thesis. Shimane Un Salters, V. & Stracke, A. 2004. Composition of depleted mantle, Geochem, Geophys. Geos 5 (5), 27 pp..
Saunders, A.D., Norry, M.J., Tarney, J., 1988. Origin of MORB and chemically depleted mantle reservoirs: trace element constraints. J. Petrology. Special Lithosphere Issue 415–445.
Shibata, T., Nakamura, E., 1997. Across-arc variations of isotope and trace element compositions from Quaternary basaltic volcanic rocks in northeastern Japan: implications for interaction between subducted oceanic slab and mantle wedge. J. Geophys. Res. 102, 8051–8064.
Sierra, G., 1994. Structural and Sedimentary Evolution of the Irra Basin, Northern Colombian Andes. Master Thesis, Department of Geological Science. State University of New York, Binghamton, NY, p. 102 pp..
Sierra, G.M., Marín Cerón, M.I., 2011. Petroleum Geology of Colombia. Amagá, Cauca and patía basins. Agencia Nacional de Hidrocarburos 104.
Silva, J.C., Sierra, G.M., Correa, L.G., 2008. Tectonic and climate driven fluctuations in the stratigraphic base level of a Cenozoic continental coal basin, northwestern Andes. J. S. Am. Earth Sci. 26, 369–382.
Singer, B.S., Dungan, M.A., Layne, G.D., 1995. Textures and Sr, Ba, Mg, Fe, K, and Ti compositional profiles in volcanic plagioclase: clues to the dynamics of calc-alkaline magma chambers. Am. Mineral. 80, 776–798.
Stern, C.R., 2004. Active Andean volcanism: its geologic and tectonic setting. Andean Geol. 31 (2), 161–206.
Sun, S.-s., McDonough, W.F., 1989. Chemical and Isotopic Systematics of Oceanic Basalts: Implications for Mantle Composition and Processes, 4.D. Saunders. In: Norry, M.J. (Ed.), Magmatism in the Ocean Basins. Geological Society, London, 3 13-345.
Taboada, A., Rivera, Luís A., Fuenzalida, A., Cisternas, A., Philip, Hervé, Bijwaard, H., Olaya, J., Rivera, C., 2000. Geodynamics of the northern Andes: subductions and intracontinental deformation (Colombia). Tectonics 19 (5), 787–813.
Tamura, Y., Nakamura, E., 1996. The arc lavas of the Shirahama Group Japan: Sr and Nd isotopic data indicate mantle-derived bimodal magmatism. J. Petrol. 37 (6), 1307–1319.
Tassinari, C.C.G., Díaz, F., Buena, J., 2008. Age and sources of gold mineralization in the Marmato mining district, NW Colombia: a Miocene – Pliocene epizonal gold deposit. Ore Geol. Rev. 33, 505–518.
Tatsumi, Y., 2005. The subduction factory: how it operates in the evolving earth. GSA Today (Geol. Soc. Am.) 15 (7), 4–10.
Tatsumi, Y., Stern, R.J., 2006. Manufacturing continental crust in the subduction factory. Oceanography 19 (4), 104–112.
Tatsumi, Y., Takahashi, T., 2006. Operation of the subduction factory and production of andesite. Journal of Mineralogical and Petrographical Sciences 101, 145–153.
Thorpe, R.S., 1984. The tectonic setting of active Andean volcanism. In Andean magmatism: chemical and Isotopic Constraints. In: Harmon, R.S., Barreiro, B.A. (Eds.), Shiva Geological Series. Shiva Publications, Nantwich, U.K., pp. 4–8
Thorpe, R.S., Francis, P.W., 1979. Variations in Andean andesite composition and their petrogenetic significance. Tectonophysics 57, 53–70.
Thorpe, R.S., Francis, P.W., Hammill, M., Baker, M.C.W., 1982. The Andes. Andesites. In: Thorpe, R.S, pp. 187–205.
Toro, G., Restrepo, J.J., Poupeau, G., Saenz, E y, Azdimousa, A., 1999. Datación por trazas de fisión de circones rosados asociados a la secuencia volcano – sedimentaria de Irra (Caldas). Boletín de Ciencias de la Tierra 13, 28–34.
Trenkamp, R., Kellogg, J.N., Freymueller, J.T., Mora, H.P., 2002. Wide plate margin deformation, southern Central America and northwestern South America, CASA GPS observations. J. S. Am. Earth Sci. 15, 157–171.
Uribe – Mogollón, C.A., 2013. Hydrothermal Evolution of the Titiribí Mining District. Undergraduate Thesis. EAFIT University, p. 127 pp..
van der Hammen, T., 1960. Estratigrafía del Terciario y Maastrichtiano continentales y tectogénesis de los Andes Colombianos, Informe No. 1279. Servicio Geológico Nacional, Bogotá 128.
Vargas, C., Mann, P., 2013. Tearing and breaking off of subducted slabs as the result of collision of the Panama arc-indenter with northwestern South America. Bull. Seismol. Soc. Am. 103, 2025–2046.
Vermeesch, P., 2009. RadialPlotter: a Java application for fission track, luminescence and other radial plots. Radiat. Meas. 44, 409–410.
Walker, G.P.L., Wilson, C.J.N., Froggat, P.C., 1991. An ignimbrite veneer deposits; the trail marker of a pyroclastic flow. J. Volcanol. Geoth. Res. 9, 409–421.

Weber, M.B.I., Tarney, J., Kempton, P.D., Kent, R.W., 2002. Crustal make-up of the northern Andes: evidence based on deep crustal xenolith suites, Mercaderes, SW Colombia. Tectonophysics 345, 49–82.
White, W.M., 2013. Geochemistry, first ed. Wiley-Blackwell, Hoboke, NJ, p. 660 pp..
White, W.M., Dupre, B., Vidal, P., 1985. Isotope and trace element geochemistry of sediments from the Barbados ridge – demerara plain region, atlantic ocean. Geochem. Cosmochim. Acta 49, 1875–1886.
Wilson, M., 1989. Igneous Petrogenesis: a Global Tectonic Approach. Chapman & Hall, London, UK, p. 466 pp..
Winter, J.D., 2001. Introduction to Igneous and Metamorphic Petrology. Upper Saddle River, New Jersey. Prentice Hall, p. 796 pp..
Wörner, G., Davidson, J., Moorbath, S., Turner, T.L., McMillan, N., Nye, C., López-Escobar, L., Moreno, H., 1988. The Nevados de Payachata volcanic region 18°S/69°W, northern Chile. I. Geological, geochemical and isotopic observations. Bull. Volcanol. 30, 287–303.